NASA Technical Paper 1226

Boundary-Layer Separation on Isolated Boattail Nozzles

William Kelly Abeyounis

AUGUST 1978

NASA

NASA Technical Paper 1226

Boundary-Layer Separation on Isolated Boattail Nozzles

William Kelly Abeyounis
Langley Research Center
Hampton, Virginia

NASA
National Aeronautics
and Space Administration

Scientific and Technical Information Office

1978

SUMMARY

An investigation has been conducted in the Langley 16-foot transonic tunnel to study the phenomenon of separated flow on a series of circular-arc afterbodies. This investigation was conducted at free-stream Mach numbers from 0.40 to 0.95 at an angle of attack of 0°. Both high-pressure air and solid circular cylinders with the cylinder diameter equal to the nozzle-exit diameter were used to simulate jet exhausts. A detailed data base of boundary-layer separation locations was obtained by using oil-flow techniques.

Results of this investigation indicated that boundary-layer separation is most extensive on steep boattails at high Mach numbers. Changes in the jet total-pressure ratio (jet total pressure to free-stream static pressure) affected the extent of separation very little; however, comparison of the separation data obtained by using the two jet-simulation techniques indicated that entrainment associated with the presence of a jet had a significant effect on the extent of separation. The predictions of eight separation criteria were evaluated by using experimental data. In general, no criterion accurately predicted the separation locations on the solid-simulator configurations. The best predictions, however, were obtained by curve-fitting a modified Reshotko-Tucker criterion with experimental data.

INTRODUCTION

The nacelle afterbody is a critical area insofar as airplane performance is concerned. The external flow close to the nacelle surface goes through an expansion, then a compression (ref. 1), and finally an interaction with the jet plume. This phenomenon causes the afterbody boundary layer to thicken and, in many cases, separate. As would be expected, the pressure distribution and drag on the afterbody greatly differ for cases in which boundary-layer separation does occur than for cases in which there is no separation (ref. 1). Since the flow in this region is so complex, its characteristics are hard to predict. This fact has led to much experimental work in the area (refs. 1 to 9); however, little detailed separation-location data are available from which improved analytical techniques can be developed.

Presently, there are many theoretical and semiempirical methods for predicting afterbody flows (refs. 9 to 33). Most of these employ a potential flow calculation coupled with a boundary-layer calculation. Some of the boundary-layer methods are designed to predict and calculate separated flows implicitly. Others approach the problem by predicting the separation location using simpler, semiempirical techniques (refs. 34 to 52) and modeling the separated region as a solid cone frustum (ref. 37). Good results have been obtained for unseparated boattail flows (ref. 1). For separated flows, however, the difficulty in correctly modeling the complex flow near afterbodies has heretofore caused inaccurate theoretical predictions.

In order to better understand boattail flow separation and to determine the best separation criteria for use in patched inviscid/viscid interaction solutions, an oil-flow study was conducted in the Langley 16-foot transonic tunnel in which a series of circular-arc afterbodies (ref. 1) were used. The tests were conducted at free-stream Mach numbers from 0.40 to 0.95 at an angle of attack of 0°. Air was used to simulate jet exhausts with jet total-pressure ratios (jet total pressure to free-stream static pressure) varying from jet-off up to about 9, depending upon the configuration and the free-stream Mach number. Solid cylinders were also used to simulate the jets at the on-design condition. (The flow conditions for which pressure data were available in refs. 1 to 3 were repeated as closely as possible during the present oil-flow tests.) The primary purpose of the investigation was to establish a systematic data base from which the dependency of flow separation on such factors as free-stream Mach number, longitudinal surface curvature, and jet total-pressure ratio could be determined. (Since a single model was used and since the tunnel is atmospheric, it was possible to test over only a limited range of Reynolds number. For this reason, the effect of Reynolds number was not included in the data base.) The experimental results are reported herein, and an evaluation of several of the semiempirical techniques for predicting flow separation is also presented.

The information presented in this paper was offered as a thesis in partial fulfillment of the requirements for the Degree of Master of Science, George Washington University, Washington, D.C., May 1977.

SYMBOLS

A cross-sectional area, cm^2

a intercept of linear least-squares curve

b slope of linear least-squares curve

C constant in Stratford criterion (see eq. (6))

C_f local skin-friction coefficient, τ_w/q_ℓ

C_p pressure coefficient based on free-stream conditions, $\dfrac{p_\ell - p_\infty}{q_\infty}$

$C_{p,o}$ pressure coefficient based on conditions at minimum static pressure on boattail, $\dfrac{p_\ell - p_o}{q_o}$

$C_{p,S}$ modified pressure coefficient in Stratford criterion, $1 - \left(\dfrac{M_\ell}{M_o}\right)^2$

d diameter, cm

E standard error of estimate, $\sqrt{\sum_{k=1}^{n} \frac{\left[y_k - (a + bz_k)\right]^2}{n - 2}}$

$\dot{I}$ momentum of entrained mass flow in Presz criterion, N

l length of boattail, cm

M Mach number

$\dot{m}$ entrained mass flow in Presz criterion, kg/sec

N_{Re} Reynolds number, $u_\infty d_m/\nu_\infty$

n number of points in linear least-squares curve (see eq. (11))

p pressure, Pa

q dynamic pressure, Pa

R boattail circular-arc radius, cm

r radial distance from center line of model, cm

S nozzle convergence length, cm (see fig. 6)

s streamwise distance along body, cm

T temperature, K

t nozzle throat length, cm

u velocity component in s-direction, m/sec

X axial distance aft from model nose, cm

x axial distance aft from start of boattail, cm (see fig. 6)

x_i axial coordinate in nozzle convergence section, cm (see fig. 6)

y dependent variable in linear least-squares curve (see eq. (11))

z independent variable in linear least-squares curve (see eq. (11))

β terminal boattail angle, deg

β_c boattail chord angle, deg

γ specific-heat ratio

Δx	axial distance from boattail minimum static-pressure point to boundary-layer separation point, $x_{sep} - x_o$, cm
δ	boundary-layer thickness, cm
δ^*	boundary-layer displacement thickness, cm
θ	boundary-layer momentum thickness, cm
ν	kinematic viscosity, m^2/sec
ρ	density, kg/m^3
τ_w	wall shear stress, N/m^2

Subscripts:

b	base
cav	cavity
DP	dew point
e	exit
eff	effective
fs	fictitious stagnation point
j	jet
ℓ	local
m	maximum
o	boattail minimum static-pressure point
p	predicted
ps	preseparation
s	plume simulator
sep	separation point
t	stagnation
1	boundary-layer edge, top edge of control volume in Presz criterion
∞	free stream

EXPERIMENTAL APPARATUS AND PROCEDURE

Wind Tunnel

This flow-separation study was conducted in the Langley 16-foot transonic tunnel. The tunnel is a single-return, continuous-flow, atmospheric tunnel. The free-stream Mach number is continuously variable from 0.20 to 1.30. A more detailed description of the Langley 16-foot transonic tunnel can be found in references 53 to 55.

Model and Support System

The model used in this investigation was an isolated, single-engine nacelle model, to which various circular-arc boattail nozzles could be attached. A sketch of a typical configuration, in which high-pressure air was used to simulate the jet exhaust, is shown in figure 1. The nacelle model had a rounded shoulder at the junction of the conical nose and the cylindrical section to alleviate flow turbulence which would occur with a sharp corner. The nozzles were attached at station 111.76 cm. Nozzle boattails for all configurations started at station 121.92 cm. The dry, high-pressure air used for jet simulation had a stagnation temperature of about 274 K. It was piped through the model sting-strut support into the high-pressure plenum. The air then flowed radially outward (perpendicular to the model axis) into the low-pressure plenum through eight multiholed sonic nozzles equally spaced around the circumference of the high-pressure plenum. The jet simulation flow then accelerated rearward, passing through screens in the model tailpipe to smooth the flow. Figure 2 is a photograph of the air-powered model installed in the Langley 16-foot transonic tunnel.

Solid cylinders were also used to simulate jet exhausts. Figure 3 illustrates a configuration typical of those tested. An internal sting was installed in the single-engine nacelle model to support the solid simulators. Figure 4 shows one of these configurations installed in the Langley 16-foot transonic tunnel. Only simulators with a diameter equal to the nozzle exit diameter (d_s/d_e = 1.00) were tested. All simulators were 27.94 cm long. It was assumed this was long enough so that base effects of the simulator would be negligible on the boattails.

The model was mounted in the tunnel on a sting-strut support system. As shown in figures 1 to 5, the nose of the model was attached to the strut blade. The blade was swept 45° and was 5 percent thick with a 50.80-cm chord. The sting was 5.08 cm by 10.16 cm in cross section, with the top and bottom capped with half-cylinders of 2.54-cm radius. The center line of the sting was 55.88 cm below the wind-tunnel center line. This placed the axis of the model on the tunnel center line, with the nose of the model at tunnel station 39.93 m. Cross-sectional area distributions of the model and support system are shown in figure 5. The model cross-sectional area was 0.099 percent of the cross-sectional area of the test section; the maximum cross-sectional area of the model and support system was 0.148 percent.

Afterbody Models

A family of eight circular-arc afterbodies was tested. Figure 6 shows sketches and corresponding tables of dimensions for these nozzle afterbodies. The internal contour of each nozzle was basically an ASME long-throat nozzle (ref. 56). Some modifications were necessary because the external contours set limits within which the internal contours had to contract from a fixed internal diameter to the required exit diameter. Also, space had to be allotted for tube routing. All of the nozzles had throats with circular cross sections.

Instrumentation and Test Procedure

The eight afterbody models and their solid simulators were equipped with static-pressure orifices. The orifice locations and static-pressure data used in this paper were presented in reference 1. For those cases in which air was used to simulate jet exhausts, jet total-pressure measurements were obtained by using an internally mounted total-pressure rake (fig. 6). The jet total pressures were measured by using electrical strain-gage pressure transducers calibrated to an accuracy of ±0.5 percent of the gage capacity (689 kPa).

All testing was conducted in the Langley 16-foot transonic tunnel at free-stream Mach numbers ranging from 0.40 to 0.95 and at an angle of attack of 0°. The tunnel upflow (on the order of 0.1° throughout the free-stream Mach number range) and sting deflection (known to be extremely small) were not taken into account. By use of the techniques described in references 57 and 58, boundary-layer transition was fixed by a 0.254-cm strip of No. 100 grit, located 2.54 cm from the tip of the nose.

High-pressure air was used to simulate jet exhausts, with jet total-pressure ratios varying from jet-off ($p_{t,j}/p_{\infty} = 1$) up to 9, depending upon the configuration and free-stream conditions. This range in jet total pressure covers that typically used in subsonic flight by transports and fighters.

Since the Langley 16-foot transonic tunnel is an atmospheric tunnel, the tunnel free-stream conditions vary with the ambient conditions. The range of free-stream conditions is shown as a function of free-stream Mach number in figure 7.

For the purpose of obtaining oil-flow data, the aft portion of the model was painted with 100-weight oil before each run and was repainted as often as necessary to insure good oil-flow quality. In order to check for hysteresis, some conditions were repeated during a run (going up and coming down in Mach number).

Data Reduction

Separation locations were obtained from the oil-flow photographs. A photograph of a grid held next to the model before a run was used to scale distances. Separation distances were measured at the top of the boattail to minimize the possibility of support-strut interference. (Because photographs were taken

from above the model, the top of the boattail appears to coincide with the model center line in the photographs of figs. 8 to 10.)

RESULTS AND DISCUSSION

Experimental Results

Typical photographs obtained during this oil-flow investigation are presented as figures 8, 9, and 10. The separation line is indicated by x_{sep} in figure 8. (The light band shown in the photographs corresponds to the cylindrical portion of the nozzle upstream of the boattail and does not indicate separation.) Generally, the separation line is curved, conforming to a series of vortices spaced around the body in the separated region. In figure 9, a typical vortex is shown in the photograph at $M_\infty = 0.90$. This phenomenon, similar to Taylor and Goertler vortices (ref. 59), is characteristic of turbulent flow and is triggered perhaps by small asymmetries in the flow. Figure 8 also shows a line in the separated region near the nozzle exit. This line indicates that a two-cell vortex pattern may exist in the separated region, at least at high jet total-pressure ratios.

Some factors influencing the location of the separation point are the free-stream Mach number, the longitudinal curvature of the model, and the jet entrainment and plume blockage. The Reynolds number also affects the separation location; however, it was not possible to test over a wide range of Reynolds number since the tunnel is an atmospheric tunnel and only one model was used in the test.

Effect of Mach number.- For subsonic flow, the separation point moved forward on a given configuration as the free-stream Mach number increased. (See figs. 9 and 11.) For transonic flows (free-stream Mach numbers above about 0.8, depending upon the configuration), pressure distributions indicate that a shock probably existed on the boattail when the flow decelerated from supersonic to subsonic speeds (ref. 1). When this happened, the boundary-layer separation probably became shock induced. The separation point moved forward on the boattail to a point in the vicinity of the shock. It is speculated that the shock-induced separated region combined with the previously described separated region to cause this movement, which, in turn, may explain the large shifts in the separation location at transonic speeds that occurred for two of the configurations. (See fig. 11.)

Effect of longitudinal curvature.- The longitudinal curvature of the boattail also greatly affected the separation location. As expected, for a given free-stream Mach number, the most forward separation location occurred on the steepest boattail configuration. (See fig. 11.) As the longitudinal curvature progressively decreased from configuration to configuration, the separation location moved rearward. No separation was found on the four boattail configurations with the largest curvatures over the range of free-stream Mach number tested.

Effect of jet.- The jet entrainment and plume shape are functions of the jet total-pressure ratio. It is seen in figures 10 and 12 that the separation

location changed little over the range of jet total-pressure ratio tested. (The level of some of the data curves may be in error by as much as 0.05 for x_{sep}/d_m because of an excess of oil on the model. The data in question are at the free-stream Mach numbers of 0.84 for configuration 1, 0.84 and 0.40 for configuration 2, and 0.94 for configurations 4 and 6.) The flatness of the curves probably indicates that the changes induced in entrainment and plume-blockage effects by varying the jet total-pressure ratio were nearly equal in magnitude and opposite in effect.

Jet entrainment.- The jet entrainment tends to move the separation location rearward on the boattail by entraining mass from the separated region rearward into the jet. The magnitude of entrainment is a function of both the velocity difference and "surface" area between flows. Therefore, for a convergent nozzle with a given free-stream condition, the mass entrained into the jet would tend to increase as the jet-exit Mach number increased. This increase in jet-exit Mach number corresponds to an increase in the nozzle total-pressure ratio. If the jet velocity is less than the external velocity, the external flow actually tends to entrain mass from the jet. Also, some mixing occurs since the external flow contacts the jet flow at an angle and must be turned by the jet flow. When the on-design condition is reached, the jet-exit Mach number equals 1 and remains constant for higher jet total-pressure ratios. Consequently, the entrainment tends to level off. The entrainment does increase slightly for higher jet total-pressure ratios though, since the flow in the jet plume becomes supersonic.

Plume blockage.- While entrainment tends to move the separation location rearward, plume-blockage effects of jets tend to increase the surface static pressure of the boattail and move the separation location forward. As the jet total-pressure ratio is increased up to the on-design condition, the separation location moves rearward. As higher total-pressure ratios are reached, the plume-blockage effects increase, halting the rearward movement of the separation location and eventually causing a slight forward movement. There appears to be a disparity in some of the jet-off data which may, in part, be due to the unsteadiness that can occur in base flow conditions. Also, at the higher Mach numbers, the separation location is more sensitive to small errors in setting the Mach number in the wind tunnel.

Effect of Jet-Simulation Techniques

Since the separation location remains almost stationary throughout the range of jet total-pressure ratio, it seems likely that solid-simulator data could be used to estimate the jet-on separation locations. However, figure 13 shows that a difference between the solid-simulator data and the high-pressure air data exists in the separation locations obtained for on-design conditions. The jet total-pressure ratio at which the on-design condition occurs varies slightly for differing Mach numbers and configurations, causing some of the difference. However, since the separation location changes little throughout the range of jet total-pressure ratio, most of the difference in separation location between solid-simulator data and high-pressure air data must be a result of entrainment. For subsonic cases, this difference in separation locations obtained by using the two jet-simulation techniques appears to be mainly

a function of the "surface" area of the separated region washed by the jet (the region between the jet exit and the reattachment point on the plume). The extent of this "surface" area tends to correspond directly to the extent of separation on the boattail. For transonic cases, shock-induced separation probably occurs. Within experimental accuracy, the difference in the data curves reduces to almost zero. This indicates that the shock location is probably not greatly affected by entrainment.

Theoretical Results

Using this newly acquired data base, several flow-separation criteria, most of which are simple semiempirical methods, were evaluated in search of a criterion that would give reasonable predictions when integrated into a patched inviscid/viscid interaction computer program. A separation criterion could be applied in two ways: (1) it could be applied only during the first iteration of an inviscid/viscid interaction program with its predictions being used during the remaining iterations or (2) it could be applied during each iteration, thus providing an updated separation prediction for the next iteration. A separation criterion applied only during the first iteration should yield good predictions from a set of input parameters generated using theoretical inviscid pressure distributions. A criterion applied during each iteration should yield good predictions from a set of parameters generated using experimental pressure distributions. For this reason, the criteria were applied to two sets of parameters. The sets differed in that one used experimental pressure distributions as input to a boundary-layer program while the other used the theoretical inviscid pressure distributions. A potential flow calculation (ref. 11) and a Reshotko-Tucker momentum-integral boundary-layer calculation (ref. 12) were used to calculate the needed boundary layer and inviscid flow parameters.

There were several advantages in using the inviscid pressure distributions. The inviscid pressure distributions do not contain the scatter inherent in experimental data, and they are easily calculated. This experimental scatter (especially in the minimum pressure) can cause large deviations in the separation predictions of some criteria. Also, a criterion based on the inviscid pressure distribution could provide a simpler, noninteractive, and cheaper solution. On the other hand, a criterion based on experimental data might be more useful in an iterative scheme to solve a flow field where the separation location is continually being recalculated.

Reshotko-Tucker criterion.- One separation criterion was the Reshotko-Tucker criterion (ref. 49)

$$\frac{M_{sep}}{M_o} = 0.762 \tag{1}$$

This criterion (eq. (1)) states that the ratio of the Mach number at separation to the Mach number at the minimum pressure point is a constant. It is derived by applying the momentum and moment-of-momentum integral equations with special functions of the boundary-layer shape factor. The shear-stress terms are assumed negligible when compared with pressure terms. This criterion was

modified to better fit the present experimental data by incorporating the effect of Reynolds number through the skin-friction coefficient at the minimum pressure point $C_{f,o}$ to yield

$$\frac{M_{sep}}{M_o\sqrt[5]{C_{f,o}}} = 2.622 \tag{2}$$

In this modified form, equation (2) is hereinafter referred to simply as the Reshotko-Tucker criterion.

Page criterion.- Another criterion evaluated

$$(C_{p,o})_{sep} = \frac{p_{\ell,sep} - p_o}{q_o} = 0.38 \tag{3}$$

was the Page criterion (ref. 34). This simple criterion states that separation occurs where the pressure coefficient based on the minimum static pressure reaches 0.38.

Presz criterion.- A third method evaluated was the Presz criterion (ref. 37). The separation location was determined by using the following equations:

$$F = \frac{p_{sep}\, M_{sep}\sqrt{2 + (\gamma - 1)M_{sep}^2}\left(1 - \frac{\delta^*}{\delta}\right)_{sep}}{\left(1 + \frac{\dot{m}_1}{\dot{m}_o}\right)p_o M_o\sqrt{2 + (\gamma - 1)M_o^2}\left(1 - \frac{\delta^*}{\delta}\right)_o} \tag{4}$$

$$G = \frac{\frac{p_1 - p_{sep}}{p_o} - \gamma M_{sep}^2\frac{p_{sep}}{p_o}\left(1 - \frac{\delta^*}{\delta} - \frac{\theta}{\delta}\right)_{sep}}{\frac{p_1}{p_o} - 1 - \gamma M_o^2\left(1 - \frac{\delta^*}{\delta} - \frac{\theta}{\delta}\right)_o - \frac{\dot{I}_1}{p_o\delta_o} + \tau_w\frac{s}{p_o\delta_o}} \tag{5}$$

where

$$\dot{m}_1 = 0.03(\rho u)_1\, s\left(\frac{\delta_o - \delta_o^*}{\theta_o} - 3\right)^{-0.62}$$

$$\frac{\dot{I}_1}{p_o \delta_o} = \frac{\dot{m}_1}{\dot{m}_o}\left(1 - \frac{\delta^*}{\delta}\right)_o \gamma M_o M_1 \sqrt{\frac{2 + (\gamma - 1)M_o^2}{2 + (\gamma - 1)M_1^2}}$$

and

$$p_1 = \frac{1}{s_{sep}} \int_{s_o}^{s_{sep}} p_\ell \, ds$$

This method uses the control-volume approach. The control volume consists of a section of the boundary layer with one end at the minimum static-pressure location and the other at the separation location. Quantities with subscript 1 are conditions at the outer edge of the control volume. Equations (4) and (5) are equations for the ratio of the boundary-layer thickness at the minimum static-pressure location to that at the separation location. The ratio F is given in equation (4) as an integrated form of the continuity equation, whereas the ratio G is given in equation (5) as an integrated form of the momentum equation. Flow separation occurs when

$$F = G$$

Stratford criterion.- The Stratford criterion (refs. 36 and 38) is a well-known method for determining the separation location. Several similar existing methods were combined to form this criterion. Lahti's version of Stratford's criterion (ref. 35) was used in the evaluation as follows:

$$(C_{p,S})_{sep}\left(s_{eff} \frac{dC_{p,S}}{ds_{eff}}\right)_{sep}^{0.5}\left(N_{Re} \times 10^{-6}\right)_{sep}^{-0.1} = C \qquad (6)$$

where

$$C_{p,S} = 1 - \left(\frac{M_\ell}{M_o}\right)^2$$

and

$$s_{eff} = s - s_o + s_{fs}$$

The effect of the forebody pressure distribution and the actual boundary-layer transition location on the boundary-layer flow over the boattail is handled by computing s_{fs}, the effective distance for a flat-plate turbulent boundary layer to develop the momentum thickness at s_o. Separation is indicated when

the value of C is between 0.5 and 0.6. The separation location corresponds to the maximum value of C in this interval. The Stratford criterion assumes that the boundary layer consists of two different layers. The inner one is independent of upstream conditions, and the outer layer is assumed to be affected by only the initial velocity profile and the downstream pressure gradient.

Townsend criterion.- The Townsend criterion (refs. 39 and 52) is given by the equation

$$\log\left[\frac{u_o}{\nu}\left(\frac{ds}{dC_{p,o}}\right)_{ps} C_{f,o}\right]^{1.5} = \left[\frac{1}{2.98}\,\frac{(C_{p,o})_{sep}}{C_{f,o}} + 2.7\right]^{0.5} + \log\left\{\left[\frac{1}{2.98}\,\frac{(C_{p,o})_{sep}}{C_{f,o}} + 2.7\right]^{0.5} - 1\right\} - 2.913 \qquad (7)$$

Equation (7) is derived with the assumption that the separation is dependent upon the pressure gradient. This is incorporated into the criterion by the presence of the pressure gradient upstream of separation.

Angle criterion.- Another method used and referred to as the Angle criterion is given by the following equation:

$$M_{sep} \sin \beta_{sep} = -0.247 \qquad (8)$$

Equation (8) assumes that the separation location is a function of the local boattail angle and Mach number. It was derived by fitting a curve to the solid-simulator data of this investigation.

Goldschmied criterion.- The Goldschmied criterion (refs. 40 and 41), another well-known simple method, is

$$(C_{p,o})_{sep} = 200 C_{f,o} \qquad (9)$$

Equation (9) assumes that the boundary layer consists of two layers; it also assumes that a line of constant total pressure exists parallel to the surface. This line intersects the inner layer at the beginning of the adverse pressure gradient. Separation is assumed to occur when the laminar sublayer thickens enough to intersect the line of constant total pressure. This viscous phenomenon is correlated through the use of the skin-friction coefficient at the start of the adverse pressure gradient.

Wu criterion.- The Wu criterion (ref. 51), another simple equation, is

$$\frac{p_{sep}}{p_o} - 0.565M_o = 0.795 \qquad (10)$$

Equation (10) is based on experimental data and assumes that separation is a function of two parameters. One of these is the Mach number at the start of the adverse pressure gradient; the other is the ratio of the separation static pressure to the minimum static pressure.

Comparison of Separation Predictions and Solid-Simulator Data

The eight criteria were evaluated by comparing their separation predictions with experimental data. The conditions used in the evaluation were those for which separation was observed on the configurations with solid simulators. Figures 14 and 15 show the variation of separation location with Mach number for the various criteria. In figure 14, the experimental pressure distributions were used in the calculations; in figure 15, the theoretical inviscid pressure distributions were used. The scatter in the experimental data caused much of the scatter in figure 14. Also, because of the pressure plateau in the separated region, a small error in the value of the predicted separation pressure can result in a large error in separation location when experimental pressures are used. In fact, the Goldschmied criterion predicted separation for only four cases, and the Wu criterion failed to predict any at all. As shown in figure 15, the predicted trends using the inviscid pressure distributions were much smoother, although they were often very inaccurate. The Wu criterion was able to predict separation for only five cases. In general when the inviscid pressure distribution was used, the Goldschmied criterion predicted the most rearward separation locations. It was followed in order by the predictions of Page, Reshotko-Tucker, Townsend, Presz, and Stratford. The best overall predictions were made by using the Angle criterion based on experimental pressure distributions. (See fig. 14.) This was not surprising since the same data were used to derive the Angle criterion. However, none of the criteria appeared to provide very accurate results.

The inaccuracy of the predictions is better seen in figures 16 and 17. In figure 16, the predicted separation locations based on the experimental pressure distributions are plotted as a function of the experimental separation locations. The predictions based on the inviscid pressure distributions are plotted in figure 17. (The limited results of the Wu criterion and the Goldschmied criterion based on the experimental pressure distributions are not presented.) The minimum static pressures and their locations are listed in table I. The extent to which the predictions deviate can be seen for all criteria. It should be noted, however, that some of the scatter seen in both figures 16 and 17 is due to the experimental error in the oil-flow data itself. By comparing the standard error of estimate

$$E = \sqrt{\sum_{k=1}^{n} \frac{\left[y_k - (a + bz_k)\right]^2}{n - 2}} \tag{11}$$

for each criterion, the Angle criterion based on the experimental pressure distributions was found to yield the best results (E = 0.073). The next best results were obtained by using the Reshotko-Tucker criterion based on the inviscid pressure distributions.

It is also seen in figures 16 and 17 that the results based on the inviscid pressure distributions are more linear. By fitting a least-squares curve, that is, by treating the predictions as a linear function of the experimental data, an improved prediction can be obtained empirically. The standard errors of estimate (eq. (11)) of the resulting curve fits are as follows:

Criterion	E
Reshotko-Tucker	0.038
Page	0.041
Presz	0.047
Stratford	0.048
Townsend	0.051
Angle	0.058
Goldschmied	0.062

The improved results obtained by applying the curve fit to the Reshotko-Tucker criterion are compared with the oil-flow data in figure 18. The least-squares equation for this criterion is

$$\frac{x_{sep}}{d_m} = 1.870\left(\frac{\Delta x}{d_m}\right)_p - 0.388 + \frac{x_o}{d_m} \tag{12}$$

where x_o/d_m is the minimum pressure location, $\left(\Delta x/d_m\right)_p$ is the original predicted separation location, and x_{sep}/d_m is the improved prediction. It is seen that the accuracy can significantly be improved by using this technique. Although equation (12) predicts well the separation locations of this data base, its predictions for other configurations and Reynolds numbers may not be accurate.

The results of applying this curve-fitting technique in the prediction of pressure distributions are shown in figure 19. Inviscid theory predicts a greater expansion at the minimum pressure point and places a stagnation point at the end of the boattail. When a boundary-layer calculation is added in which the Presz cone-frustum model is used to represent the separated region, the predicted distribution more closely follows the experimental data. There are still significant errors near the minimum pressure point and near the

reattachment point on the solid simulator. The prediction near the minimum pressure point can be improved by solving the full potential flow equations (ref. 60) as the inviscid part of an inviscid/viscid interaction program. The prediction near the reattachment point requires the development of a better model of the separated flow.

CONCLUDING REMARKS

An investigation has been conducted in the Langley 16-foot transonic tunnel at an angle of attack of 0° and free-stream Mach numbers from 0.40 to 0.95 to study the phenomenon of separated flow on a series of circular-arc afterbodies. Both high-pressure air and solid circular cylinders with the cylinder diameter equal to the nozzle-exit diameter were used to simulate jet exhausts. The results indicated five primary concluding remarks:

1. The separation location moved forward with increasing longitudinal curvature.

2. The separation location moved forward with increasing free-stream Mach number. At transonic speeds, shock-induced separation probably occurred, causing the separation location to move forward to the vicinity of the shock location.

3. The separation location moved little over the range of jet total-pressure ratio from jet-off up to 9; however, there was a significant variance at subsonic Mach numbers with the solid-simulator data because of entrainment.

4. In general, none of the criteria evaluated produced accurate predictions. When the predictions were curve-fitted with experimental data, however, results were much better. Combining this curve-fitting technique with the Reshotko-Tucker criterion gave the best predictions.

5. Predicted pressure-coefficient distributions were much improved when the curve-fitting technique was used to predict the separation location. However, much better agreement with experimental data should be possible with the development of an improved separated-flow model.

Langley Research Center
National Aeronautics and Space Administration
Hampton, VA 23665
June 22, 1978

REFERENCES

1. Reubush, David E.: Experimental Study of the Effectiveness of Cylindrical Plume Simulators for Predicting Jet-On Boattail Drag at Mach Numbers up to 1.30. NASA TN D-7795, 1974.

2. Reubush, David E.: Effects of Fineness and Closure Ratios on Boattail Drag of Circular-Arc Afterbody Models With Jet Exhaust at Mach Numbers up to 1.30. NASA TN D-7163, 1973.

3. Reubush, David E.; and Runckel, Jack F.: Effect of Fineness Ratio on the Boattail Drag of Circular-Arc Afterbodies Having Closure Ratios of 0.50 With Jet Exhaust at Mach Numbers up to 1.30. NASA TN D-7192, 1973.

4. Reubush, David E.: An Experimental Investigation of Jet Plume Simulation With Solid Circular Cylinders. NASA TM X-71963, 1974.

5. Grund, E.; Presz, W., Jr.; and Konarski, M.: Predicting Airframe/Exhaust Nozzle Interactions at Transonic Mach Numbers. AIAA Paper No. 71-720, June 1971.

6. Harrington, Douglas E.: Jet Effects on Boattail Pressure Drag of Isolated Ejector Nozzles at Mach Numbers From 0.60 to 1.47. NASA TM X-1785, 1969.

7. Glasgow, E. R.; Divita, J. S.; Everling, P. C.; and Laughrey, J. A.: Analytical and Experimental Evaluation of Performance Prediction Methods Applicable to Exhaust Nozzles. AIAA Paper No. 71-719, June 1971.

8. Wu, J. M., et al.: Fundamental Studies of Subsonic and Transonic Flow Separation, Part I - First Phase Summary Report. AEDC-TR-75-95, U.S. Air Force, Sept. 1975. (Available from DDC as AD A014 802.)

9. Rom, Josef; and Bober, Lawrence J.: Calculation of the Pressure Distribution on Axisymmetric Boattails Including Effects of Viscous Interactions and Exhaust Jets in Subsonic Flow. NASA TM X-3109, 1974.

10. Flow Separation. AGARD-CP-168, Nov. 1975.

11. Hess, J. L.; and Smith, A. M. O.: Calculation of Potential Flow About Arbitrary Bodies. Progress in Aeronautical Sciences, vol. 8, D. Kuchemann, P. Carrière, B. Etkin, W. Fiszdon, N. Rott, J. Smolderen, I. Tani, and W. Wuest, eds., Pergamon Press, Inc., c.1967, pp. 1-138.

12. Users Manual for the External Drag and Internal Nozzle Performance Deck (Deck XI) - Supersonic Flow Analysis (Applicable to Deck VI). PWA-3465, Suppl. F, Pt. I (Contract No. AF33(615)-3128), Pratt and Whitney Aircraft, Sept. 1, 1968.

13. Kuhn, Gary D.: Calculation of Compressible, Nonadiabatic Boundary Layers in Laminar, Transitional and Turbulent Flow by the Method of Integral Relations. NASA CR-1797, 1970.

14. Economos, C.; and Boccio, J.: Calculation of Turbulent Boundary Layers With Heat Transfer and Pressure Gradient Utilizing a Compressibility Transformation. NASA CR-1923, 1971.

15. Hankey, W. L.: Separated Flow Studies. ARL 75-0173, U.S. Air Force, June 1975. (Available from DDC as AD A014 245.)

16. Calarese, Wladimiro: Review of Methods of Solution of Afterbody/Exhaust Nozzle Flow Fields. AFFDL-TR-74-108, U.S. Air Force, Jan. 1974. (Available from DDC as AD 787 459.)

17. Calarese, Wladimiro: Analysis of Transonic Viscous-Inviscid Interactions on Axisymmetric Afterbodies With Jet Effects and Boattail Injection in Separated Regions. AFFDL-TR-75-117, U.S. Air Force, Oct. 1975.

18. Calarese, Wladimiro: An Analytical Method To Compute Viscous-Inviscid Transonic Flow on Axisymmetric Afterbodies Including Jet Effects and Boattail Bleed in Separated Regions. AIAA Paper No. 75-1293, Sept.-Oct. 1975.

19. Cebeci, T.; and Smith, A. M. O.: A Finite-Difference Method for Calculating Compressible Laminar and Turbulent Boundary Layers. Trans. ASME, Ser. D: J. Basic Eng., vol. 92, no. 3, Sept. 1970, pp. 523-535.

20. Chow, Wen L.; Bober, Lawrence J.; and Anderson, Bernhard H.: Numerical Calculation of Transonic Boattail Flow. NASA TN D-7984, 1975.

21. South, Jerry C., Jr.; and Jameson, Antony: Relaxation Solutions for Inviscid Axisymmetric Transonic Flow Over Blunt or Pointed Bodies. AIAA Computational Fluid Dynamics Conference, July 1973, pp. 8-17.

22. Nash, J. F.; and Hicks, J. G.: An Integral Method Including the Effect of Upstream History on the Turbulent Shear Stress. Computation of Turbulent Boundary Layers - 1968 AFOSR-IFP-Stanford Conference. Volume I - Methods, Predictions, Evaluation and Flow Structure, S. J. Kline, M. V. Morkovin, G. Sovran, and D. J. Cockrell, eds., Stanford Univ., c.1969, pp. 37-45.

23. Coles, D. E.; and Hurst, E. A., eds.: Computation of Turbulent Boundary Layers - 1968 AFOSR-IFP-Stanford Conference. Volume II - Compiled Data. Stanford Univ., c.1969.

24. Altstatt, M. C.: Evaluation of a Method for Computation of Separated, Turbulent, Compressible Boundary Layers. AEDC-TR-76-27, U.S. Air Force, Feb. 1976. (Available from DDC as AD A021 090.)

25. Kuhn, Gary D.; and Nielsen, Jack N.: Prediction of Turbulent Separated Boundary Layers. AIAA Paper No. 73-663, July 1973.

26. Coles, Donald: The Law of the Wake in the Turbulent Boundary Layer. J. Fluid Mech., vol. 1, pt. 2, July 1956, pp. 191-226.

27. Stewartson, K.: Correlated Incompressible and Compressible Boundary Layers. Proc. R. Soc., ser. A, vol. 200, no. A1060, Dec. 22, 1949, pp. 84-100.

28. Gerhart, Philip M.; and Bober, Lawrence J.: Comparison of Several Methods for Predicting Separation in a Compressible Turbulent Boundary Layer. NASA TM X-3102, 1974.

29. Oswatitsch, K.: The Separation Condition of Boundary Layers. NASA TT F-15,200, 1973.

30. Sachdeva, R. C.: A Numerical Experiment on Two-Dimensional Turbulent Separation. The Aeronaut. J., vol. 76, no. 740, Aug. 1972, pp. 509-511.

31. Tsuji, Yutaka; and Morikawa, Yoshinobu: Turbulent Boundary Layer With Pressure Gradient Alternating in Sign. Aeronaut. Q., vol. XXVII, pt. 1, Feb. 1976, pp. 15-28.

32. Nash, J. F.; and Patel, V. C.: Calculations of Unsteady Turbulent Boundary Layers With Flow Reversal. NASA CR-2546, 1975.

33. Abbott, D. E.; Walker, J. D. A.; and York, R. E.: Numerical Solution of Turbulent Boundary Layers Approaching Separation. Proceedings of the Fourth International Conference on Numerical Methods in Fluid Dynamics. Volume 35 of Lecture Notes in Physics, Robert D. Richtmyer, ed., Springer-Verlag, 1975, pp. 34-39.

34. Page, R. H.: A Theory for Incipient Separation. Developments in Mechanics, Vol. 1, J. E. Lay and L. E. Malvern, eds., Plenum Press, 1961, pp. 563-577.

35. Keith, J. S.; Ferguson, D. R.; Merkle, C. L.; Heck, P. H.; and Lahti, D. J.: Analytical Method for Predicting the Pressure Distribution About a Nacelle at Transonic Speeds. NASA CR-2217, 1973.

36. Stratford, B. S.; and Beavers, G. S.: The Calculation of the Compressible Turbulent Boundary Layer in an Arbitrary Pressure Gradient - A Correlation of Certain Previous Methods. R. & M. No. 3207, British A.R.C., 1961.

37. Presz, Walter M., Jr.; and Pitkins, Edward T.: An Analytical Model of Axisymmetric Afterbody Flow Separation. AIAA Paper No. 75-65, Jan. 1975.

38. Stratford, B. S.: The Prediction of Separation of the Turbulent Boundary Layers. J. Fluid Mech., vol. 5, pt. 1, Jan. 1959, pp. 1-16.

39. Townsend, A. A.: The Behaviour of a Turbulent Boundary Layer Near Separation. J. Fluid Mech., vol. 12, pt. 4, Apr. 1962, pp. 536-554.

40. Goldschmied, Fabio R.: An Approach to Turbulent Incompressible Separation Under Adverse Pressure Gradients. J. Airc., vol. 2, no. 2, Mar.-Apr. 1965.

41. Goldschmied, Fabio R.: An Approach to Turbulent Incompressible Separation and the Determination of Skin-Friction Under Adverse Pressure Gradients. AIAA Paper No. 64-465, June-July 1964.

42. Bradshaw, P.; and Galea, P. V.: Step-Induced Separation of a Turbulent Boundary Layer in Incompressible Flow. J. Fluid Mech., vol. 27, pt. 1, Jan. 1967, pp. 111-130.

43. Robertson, James M.: Prediction of Turbulent Boundary-Layer Separation. J. Aeronaut. Sci., vol. 24, no. 8, Aug. 1957, pp. 631-632.

44. Sandborn, V. A.; and Liu, C. Y.: On Turbulent Boundary-Layer Separation. J. Fluid Mech., vol. 32, pt. 2, May 3, 1968, pp. 293-304.

45. Sandborn, V. A.; and Kline, S. J.: Flow Models in Boundary-Layer Stall Inception. Trans. ASME, Ser. D.: J. Basic Eng., vol. 83, no. 3, Sept. 1961, pp. 317-327.

46. Gadd, G. E.: Interactions Between Wholly Laminar or Wholly Turbulent Boundary Layers and Shock Waves Strong Enough To Cause Separation. J. Aeronaut. Sci., vol. 20, no. 11, Nov. 1953, pp. 729-739.

47. Ross, Donald; and Robertson, J. M.: An Empirical Method for Calculation of the Growth of a Turbulent Boundary Layer. J. Aeronaut. Sci., vol. 21, no. 5, May 1954, pp. 355-358.

48. Moses, Hal L.: The Behavior of Turbulent Boundary Layers in Adverse Pressure Gradients. Rep. No. 73 (Contract Nonr 1841(91)), Gas Turbine Lab., Massachusetts Inst. Technol., Jan. 1964. (Available from DDC as AD 438 000.)

49. Reshotko, Eli; and Tucker, Maurice: Effect of a Discontinuity on Turbulent Boundary-Layer-Thickness Parameters With Application to Shock-Induced Separation. NACA TN 3454, 1955.

50. Alber, I. E.; Bacon, J. W.; and Masson, B. S.: An Experimental Investigation of Turbulent Transonic Viscous-Inviscid Interactions. AIAA Paper No. 71-565, June 1971.

51. Wu, J. M.; Moulden, T. H.; and Uchiyama, N.: Aerodynamic Performance of Missile Configurations at Transonic Speeds Including the Effects of a Jet Plume. Tech. Rep. RD-76-23 (Contract No. DAAH01-74-C-0183), Univ. of Tennessee Space Inst., Mar. 1976. (Available from DDC as AD 027 692.)

52. Hahn, Mansop; Rubbert, Paul E.; Mahal, Avtar S.: Evaluation of Separation Criteria and Their Application to Separated Flow Analysis. AFFDL-TR-72-145, U.S. Air Force, Jan. 1973. (Available from DDC as AD 757 531.)

53. Ward, Vernon G.; Whitcomb, Charles F.; and Pearson, Merwin D.: Air-Flow and Power Characteristics of the Langley 16-Foot Transonic Tunnel With Slotted Test Section. NACA RM L52E01, 1952.

54. Schaefer, William T., Jr.: Characteristics of Major Active Wind Tunnels at the Langley Research Center. NASA TM X-1130, 1965.

55. Corson, Blake W., Jr.; Runckel, Jack F.; and Igoe, William B.: Calibration of the Langley 16-Foot Transonic Tunnel With Test Section Air Removal. NASA TR R-423, 1974.

56. Anon.: Flow Measurement by Means of Thin Plate Orifices, Flow Nozzles and Venturi Tubes. Supplement on Instruments and Apparatus, pt. 5, ch. 4, Power Test Codes, ASME, 1959, pp. 5-91.

57. Braslow, Albert L.; and Knox, Eugene C.: Simplified Method for Determination of Critical Height of Distributed Roughness Particles for Boundary-Layer Transition at Mach Numbers From 0 to 5. NACA TN 4363, 1958.

58. Braslow, Albert L.; Hicks, Raymond M.; and Harris, Roy V., Jr.: Use of Grit-Type Boundary-Layer-Transition Trips on Wind-Tunnel Models. NASA TN D-3579, 1966.

59. Schlichting, Hermann (J. Kestin, transl.): Boundary-Layer Theory. Sixth ed. McGraw-Hill Book Co., Inc., 1968.

60. Wilmoth, Richard G.: Analytical Study of Viscous Effects on Transonic Flow Over Boattail Nozzles. [Paper] 77-223, American Inst. Aeronaut. & Astronaut., Jan. 1977.

TABLE I.- MINIMUM STATIC PRESSURES AND LOCATIONS

M_∞	Experimental		Inviscid	
	x_o/d_m	$C_{p,o}$	x_o/d_m	$C_{p,o}$
	$l/d_m = 0.80$; $d_e/d_m = 0.50$			
0.40	0.1776	-0.313	0.1752	-0.345
.60	.1749	-.347	.1773	-.393
.70	.1717	-.374	.1789	-.436
.75	.1776	-.394	.1799	-.470
.80	.1742	-.423	.1813	-.517
.85	.1606	-.514	.1827	-.578
.90	.1601	-.614	.1844	-.678
.92	.1613	-.584	.1851	-.739
.94	.1675	-.547	.1858	-.828
	$l/d_m = 1.00$; $d_e/d_m = 0.50$			
0.60	0.2020	-0.271	0.2126	-0.299
.70	.2003	-.294	.2141	-.328
.75	.2003	-.310	.2151	-.351
.80	.1978	-.334	.2161	-.381
.85	.1947	-.372	.2172	-.423
.90	.2157	-.484	.2182	-.492
.92	.2615	-.489	.2184	-.527
.94	.2909	-.496	.2184	-.584
	$l/d_m = 1.00$; $d_e/d_m = 0.60$			
0.70	0.2276	-0.257	0.2208	-0.268
.75	.2230	-.272	.2218	-.286
.80	.2218	-.292	.2229	-.309
.85	.2197	-.322	.2242	-.342
.90	.2230	-.435	.2253	-.395
.92	.2994	-.441	.2256	-.425
.94	.3520	-.420	.2256	-.470
	$l/d_m = 1.00$; $d_e/d_m = 0.70$			
0.90	0.2396	-0.296	0.2335	-0.296
.92	.2314	-.355	.2340	-.319
.94	.3567	-.391	.2342	-.351

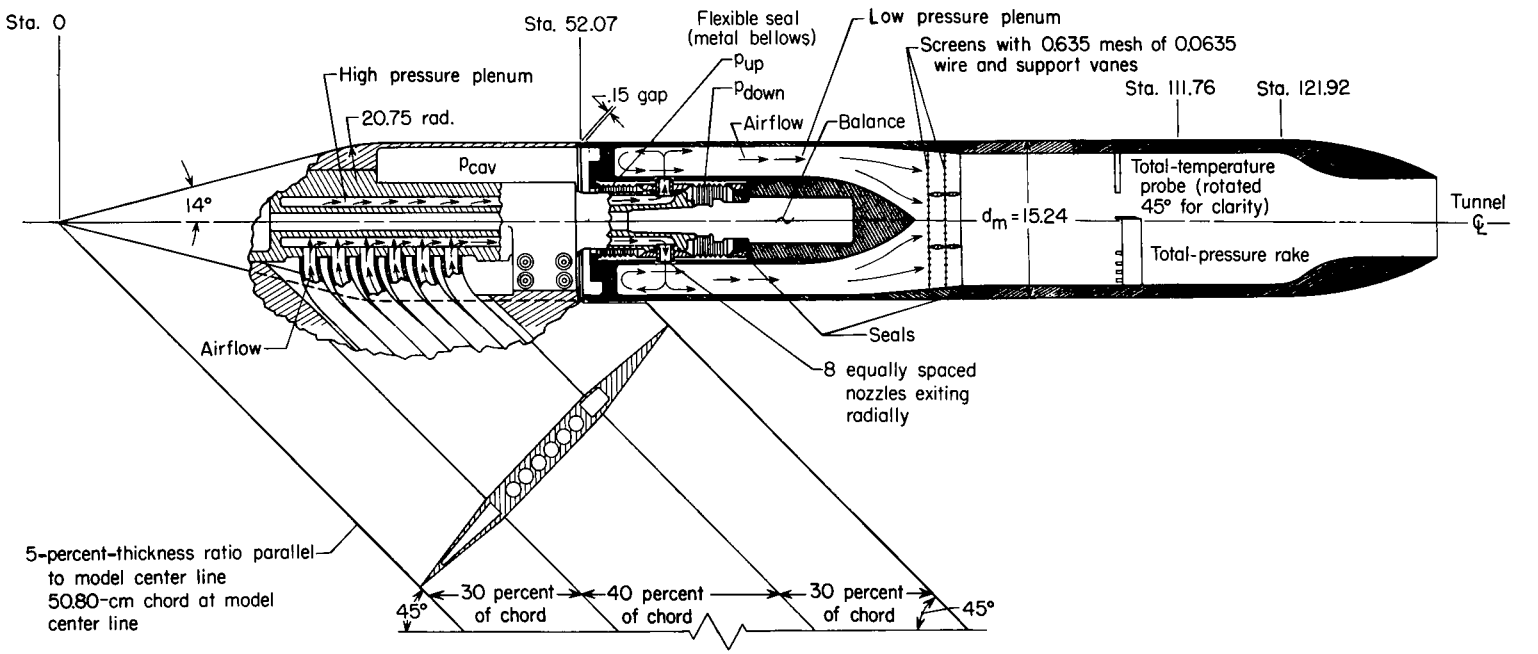

Figure 1.- Air-powered cone-cylinder model with typical circular-arc convergent nozzle installed. All dimensions are in centimeters unless otherwise noted.

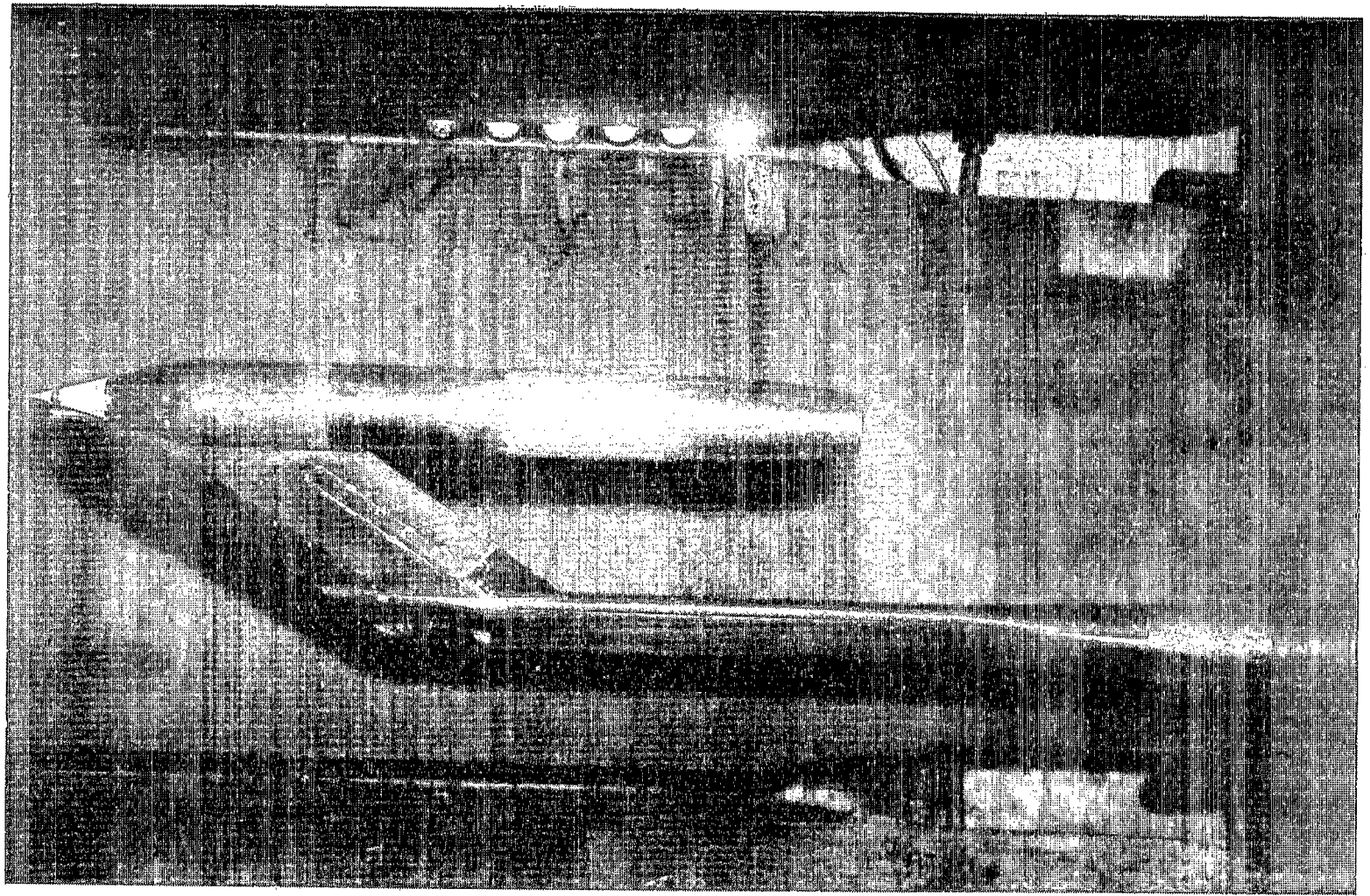

L-72-1872

Figure 2.- Air-powered model with configuration 8 attached, installed in Langley 16-foot transonic tunnel.

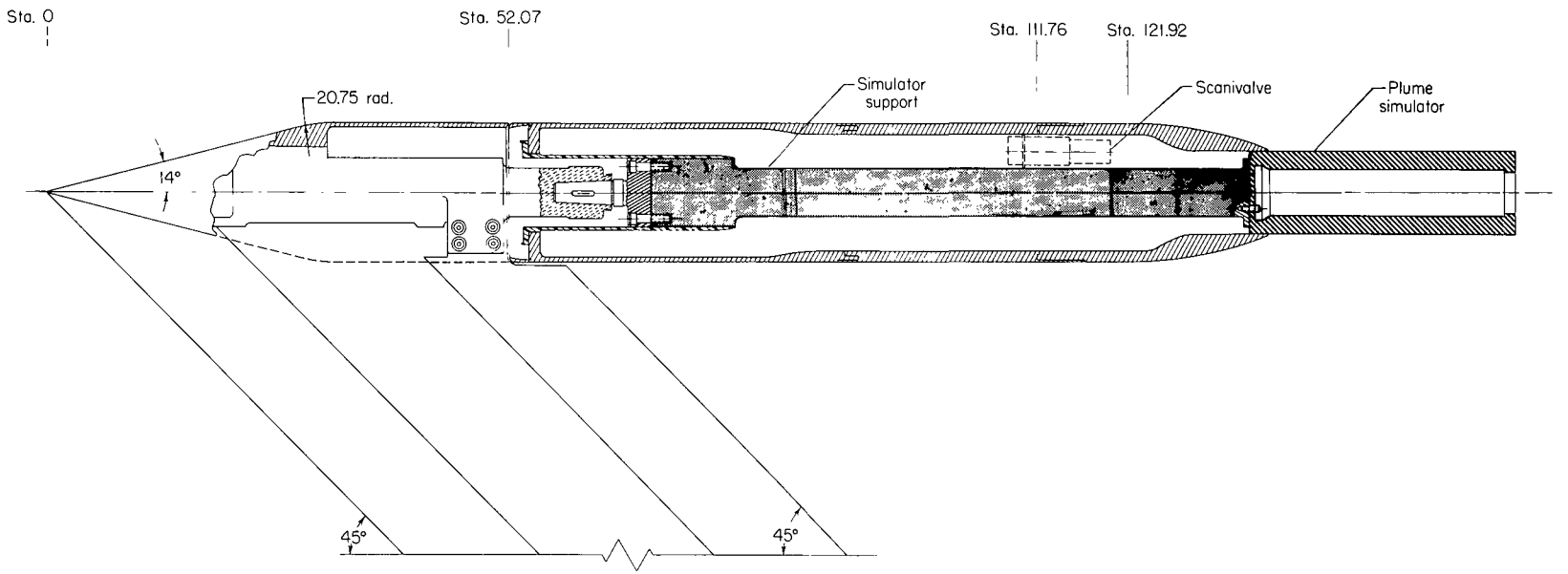

Figure 3.- Cone-cylinder nacelle model showing internal sting arrangement for support of simulators.

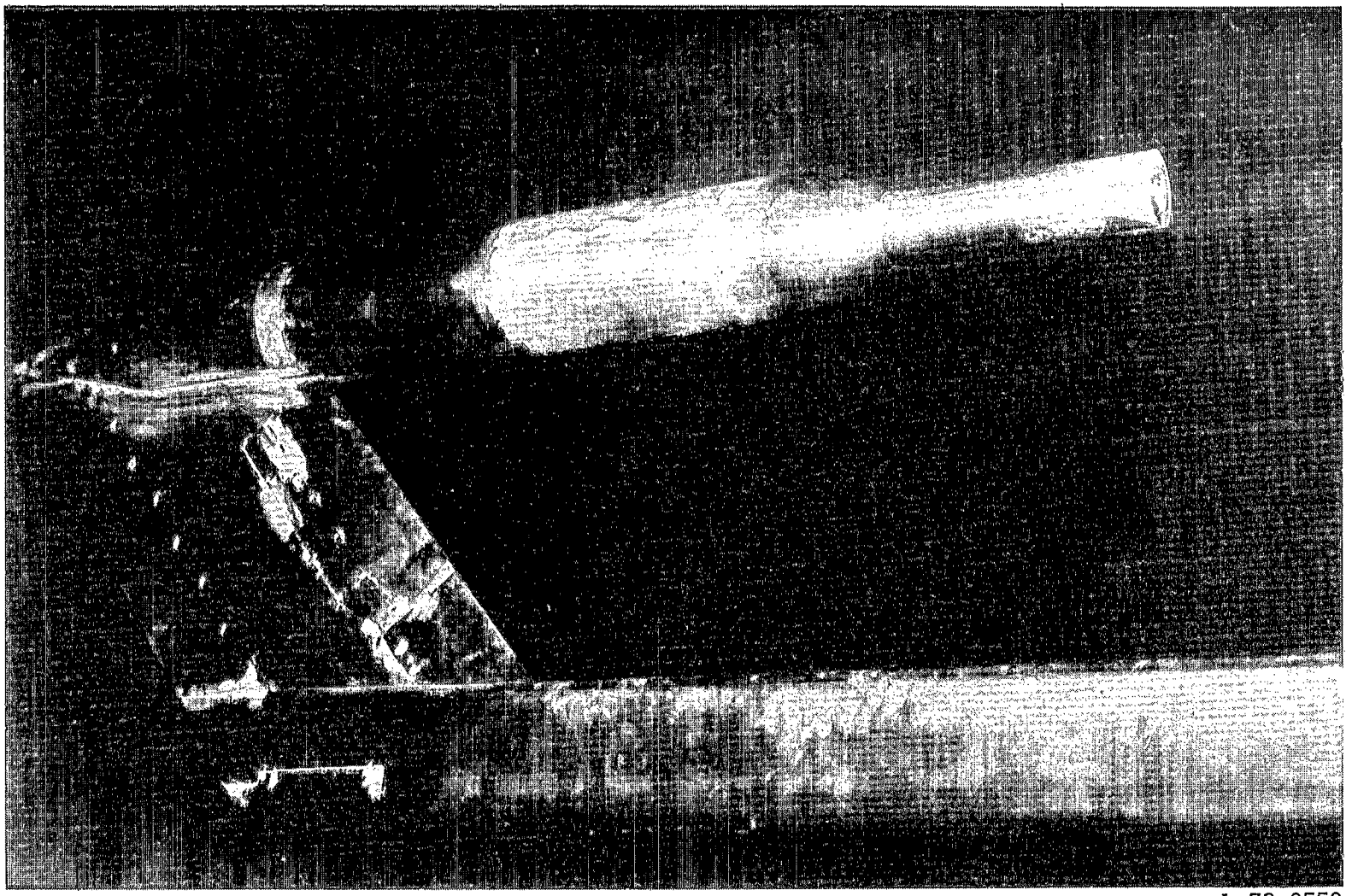

L-73-9559

Figure 4.- Nacelle model with typical circular-arc afterbody and $d_s/d_e = 1.00$ simulator attached, installed in Langley 16-foot transonic tunnel.

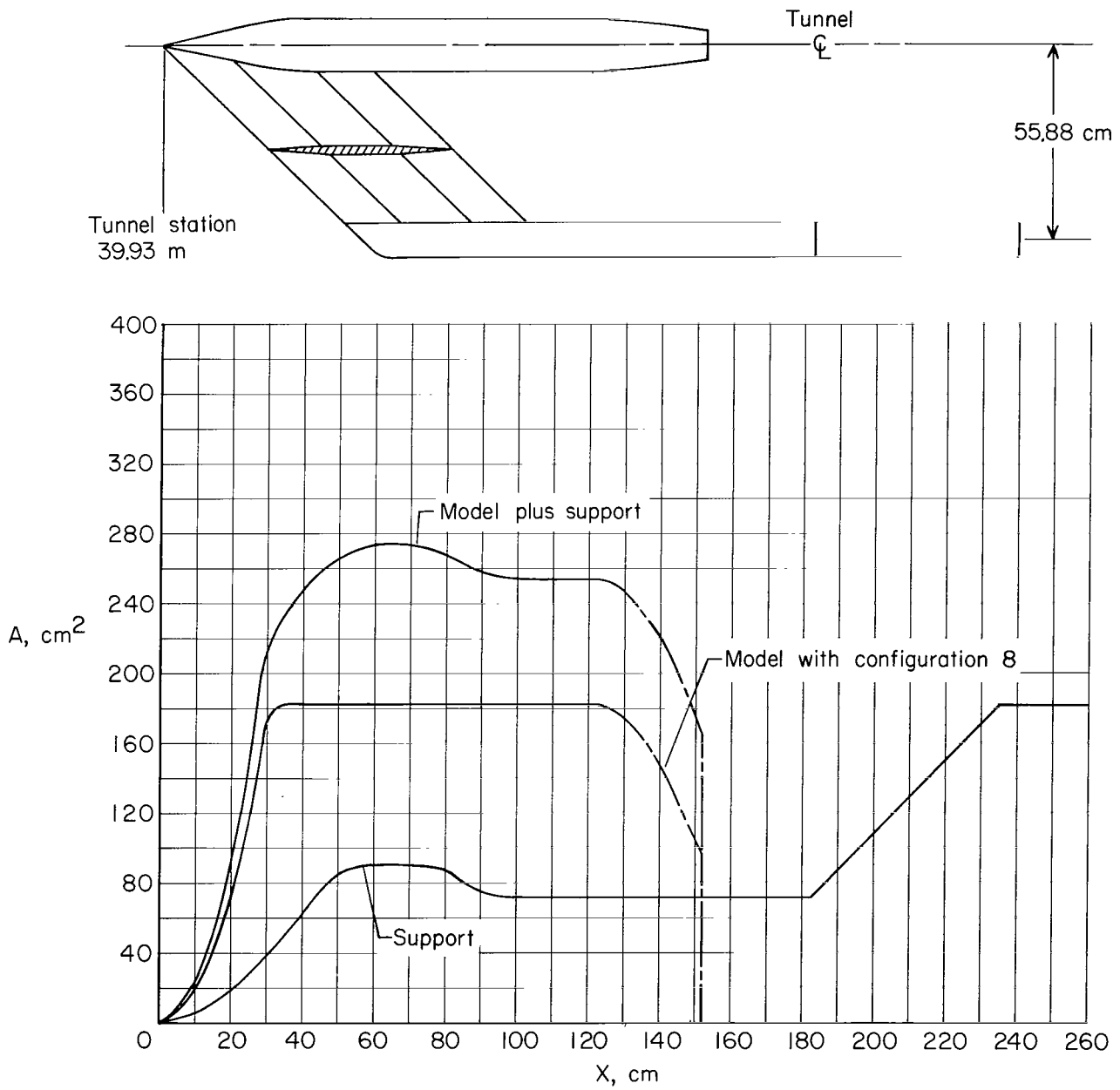

Figure 5.- Model and support system with corresponding cross-sectional area distributions.

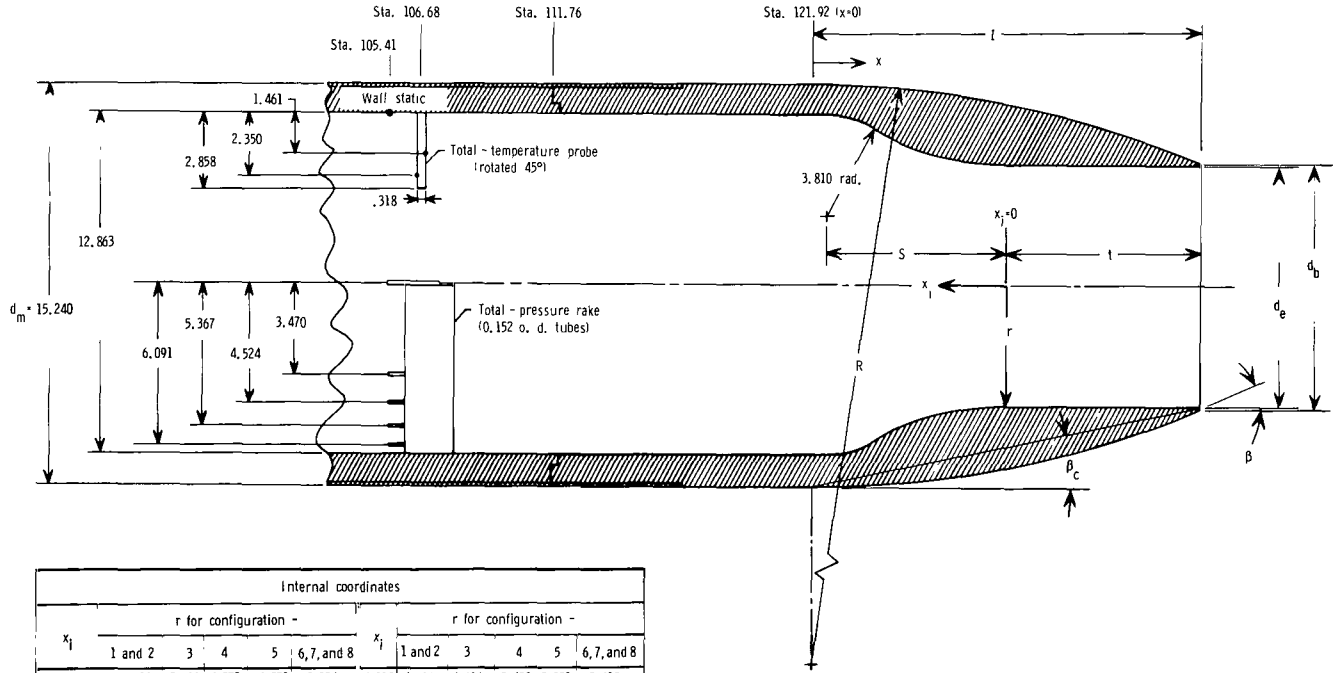

Internal coordinates											
x_i	r for configuration -					x_i	r for configuration -				
	1 and 2	3	4	5	6, 7, and 8		1 and 2	3	4	5	6, 7, and 8
0	3.810	3.810	4.572	4.572	5.334	4.318	4.696	4.696	5.458	5.052	5.618
.254	3.813	3.813	4.575	4.575	5.337	4.445	4.755	4.755	5.517	—	—
.508	3.820	3.820	4.582	4.577	5.339	4.572	4.816	4.816	5.578	5.123	5.659
.762	3.835	3.835	4.597	4.585	5.342	4.699	4.882	4.882	5.644	—	—
1.016	3.856	3.856	4.618	4.595	5.349	4.826	4.948	4.948	5.710	5.202	5.705
1.270	3.881	3.881	4.643	4.608	5.357	4.953	5.019	5.019	5.781	5.245	—
1.524	3.912	3.912	4.674	4.625	5.364	5.080	5.090	5.090	5.852	5.291	5.758
1.778	3.950	3.950	4.712	4.646	5.377	5.207	5.169	5.169	5.931	5.339	5.786
2.032	3.993	3.993	4.755	4.669	5.390	5.334	5.248	5.248	6.010	5.392	5.819
2.286	4.041	4.041	4.803	4.694	5.405	5.461	5.334	5.334	6.090	5.448	5.852
2.540	4.097	4.097	4.859	4.722	5.423	5.588	5.420	5.420	6.144	5.512	5.888
2.794	4.161	4.161	4.923	4.757	5.443	5.715	5.514	5.514	6.195	5.578	5.928
3.048	4.229	4.229	4.991	4.793	5.466	5.842	5.611	5.611	6.238	5.654	5.972
3.302	4.308	4.308	5.070	4.836	5.489	5.969	5.715	5.715	6.279	5.738	6.022
3.556	4.392	4.392	5.154	4.882	5.517	6.096	5.822	5.822	6.314	5.839	6.081
3.810	4.483	4.483	5.245	4.933	5.547	6.223	5.939	—	6.342	5.961	6.154
3.937	4.534	4.534	5.296	—	—	6.350	6.060	—	6.368	6.137	6.259
4.064	4.585	4.585	5.347	4.991	5.580	6.431	—	—	—	6.431	6.431
4.191	4.641	4.641	5.403	—	—	6.477	6.190	—	—	—	—

Geometric parameters								
Configuration	l/d_m	d_e/d_m	d_b/d_m	R/d_m	t/d_m	S/d_m	β, deg	β_c, deg
1	0.800	0.500	0.51	1.429	0.500	0.533	34.054	17.027
2	1.000	.500	.51	2.163	.500	.533	27.533	13.766
3	1.768	.500	.51	6.500	.500	.458	15.781	7.891
4	1.000	.600	.61	2.662	.500	.462	22.068	11.034
5	1.500	.600	.61	5.867	.592	.536	14.814	7.407
6	1.000	.700	.71	3.521	.367	.507	16.507	8.250
7	1.500	.700	.71	7.831	.667	.507	11.043	5.521
8	2.000	.700	.71	13.866	.833	.507	8.293	4.147

Figure 6.- Detailed sketch of typical configuration and tables of geometric parameters and internal coordinates. All dimensions are in centimeters unless otherwise noted.

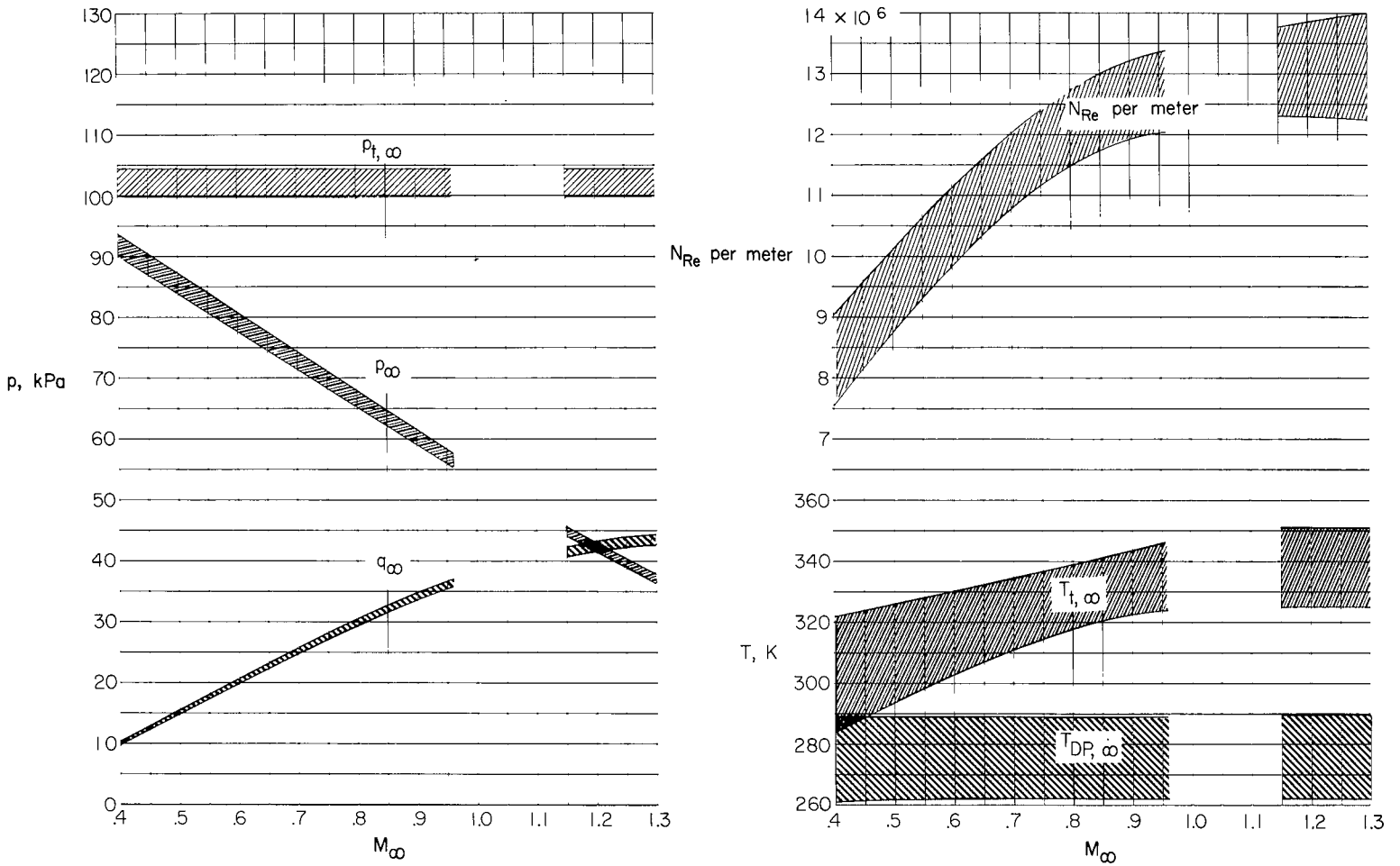

Figure 7.- Range of free-stream conditions encountered during this investigation.

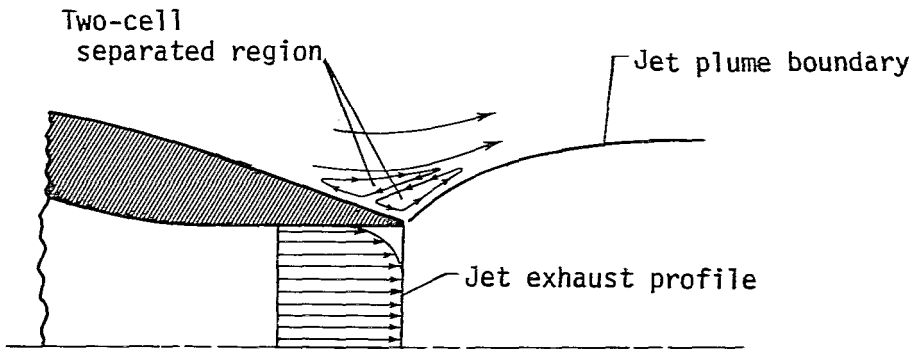

(a) Two-cell vortex model.

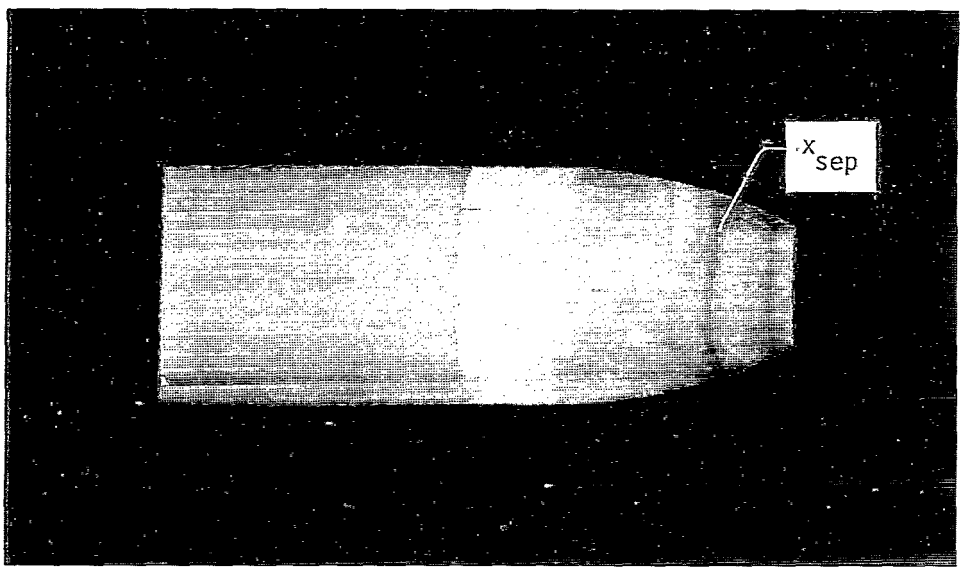

L-78-108

(b) $l/d_m = 1.00$; $d_e/d_m = 0.50$; $M_\infty = 0.90$; $p_{t,j}/p_\infty = 7.83$.

Figure 8.- Example of two-cell vortex separation.

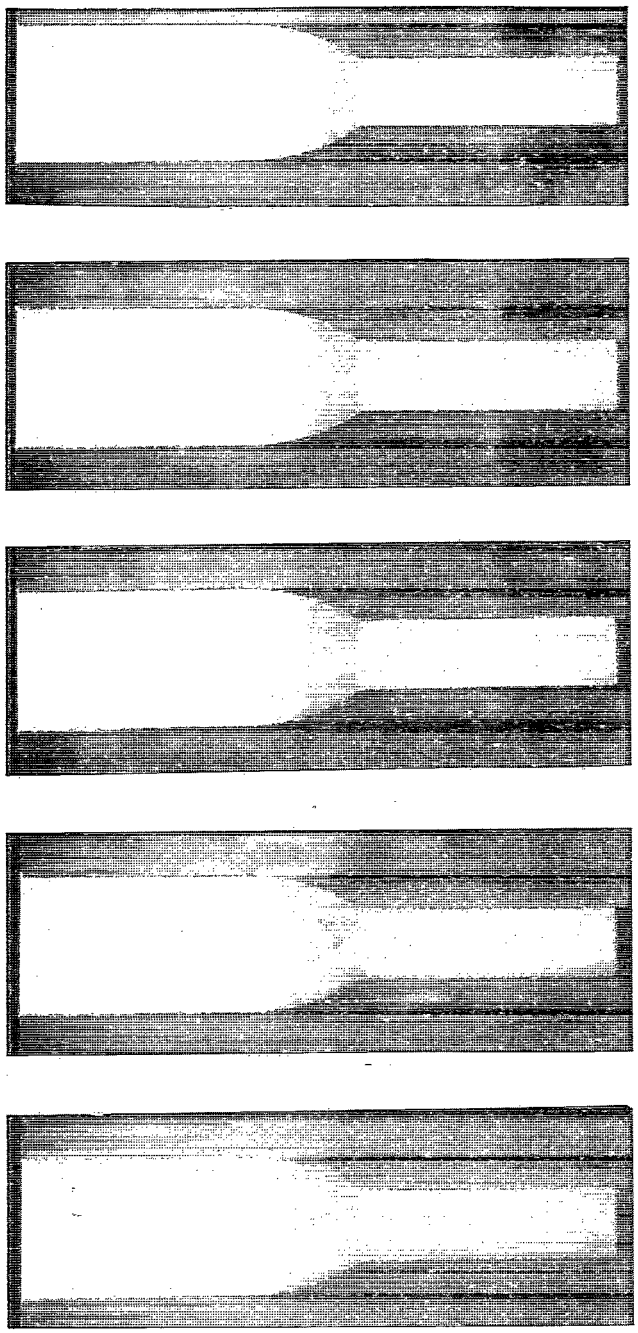

L-78-109

Figure 9.- Oil-flow photographs showing effect of Mach number on separation location. $l/d_m = 0.80$; $d_e/d_m = 0.50$.

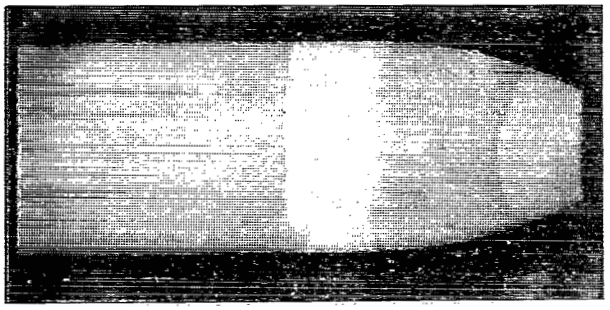

Jet off

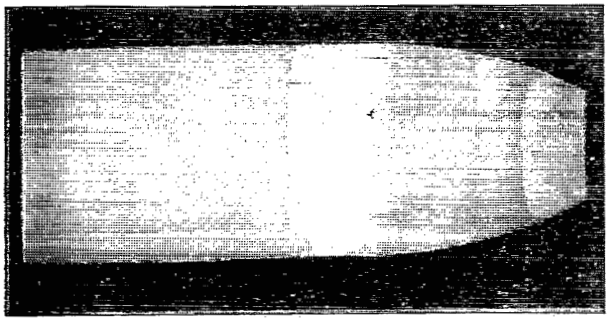

$p_{t,j}/p_\infty = 2.03$

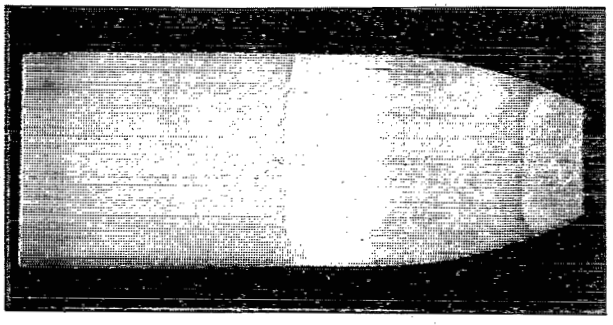

$p_{t,j}/p_\infty = 2.99$

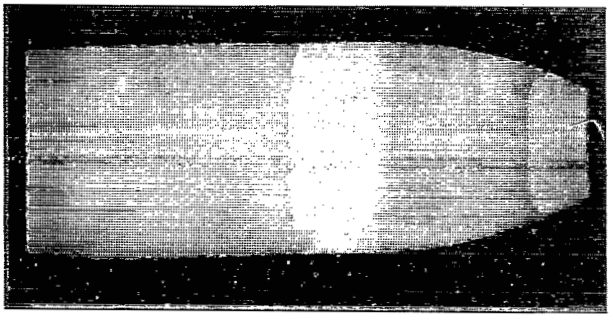

$p_{t,j}/p_\infty = 4.04$

L-78-110

Figure 10.- Oil-flow photographs showing effect of jet total-pressure ratio on separation location. $M_\infty = 0.90$; $l/d_m = 1.00$; $d_e/d_m = 0.50$.

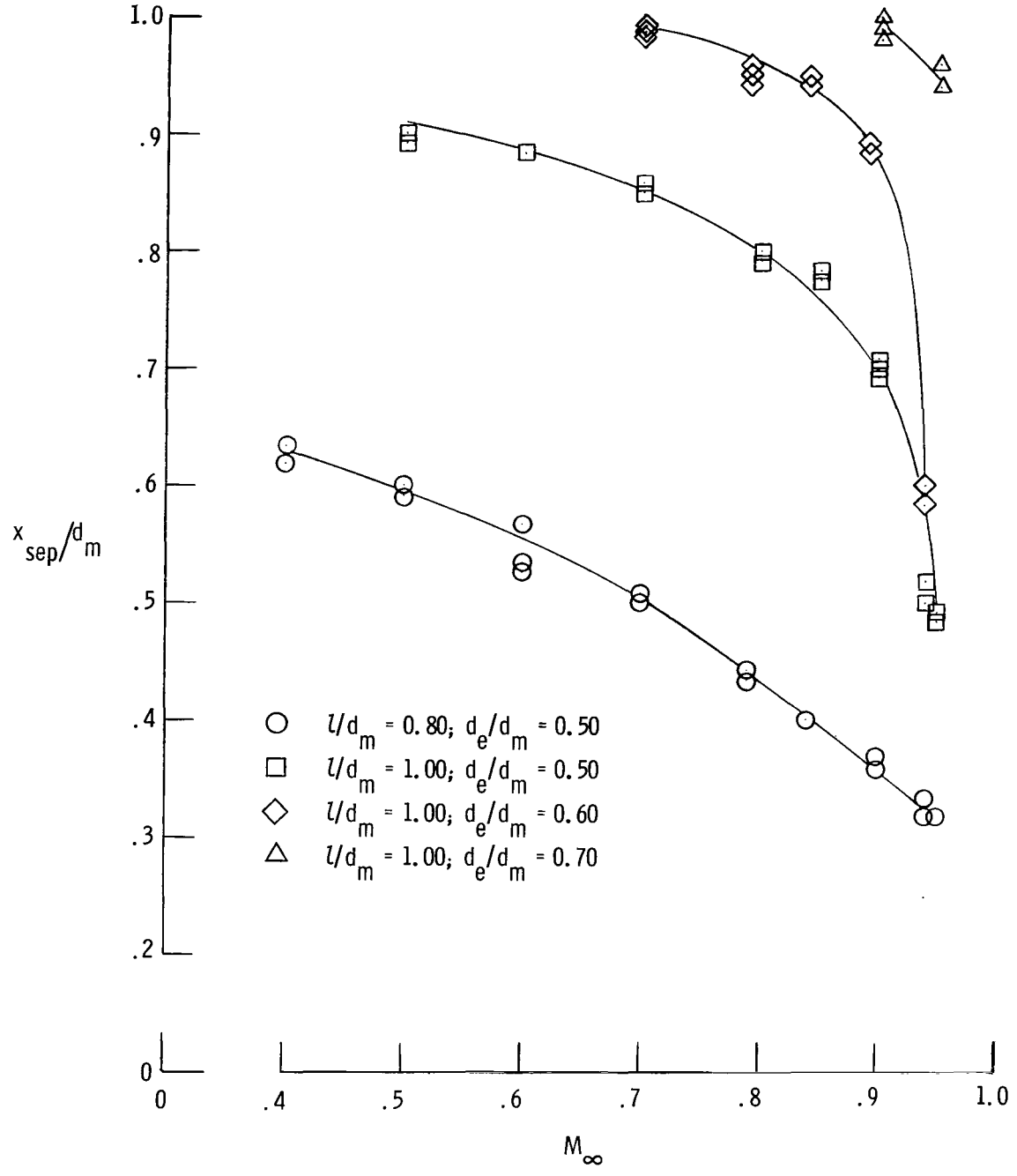

Figure 11.- Separation locations for configurations using a solid circular cylinder to simulate jet exhausts.

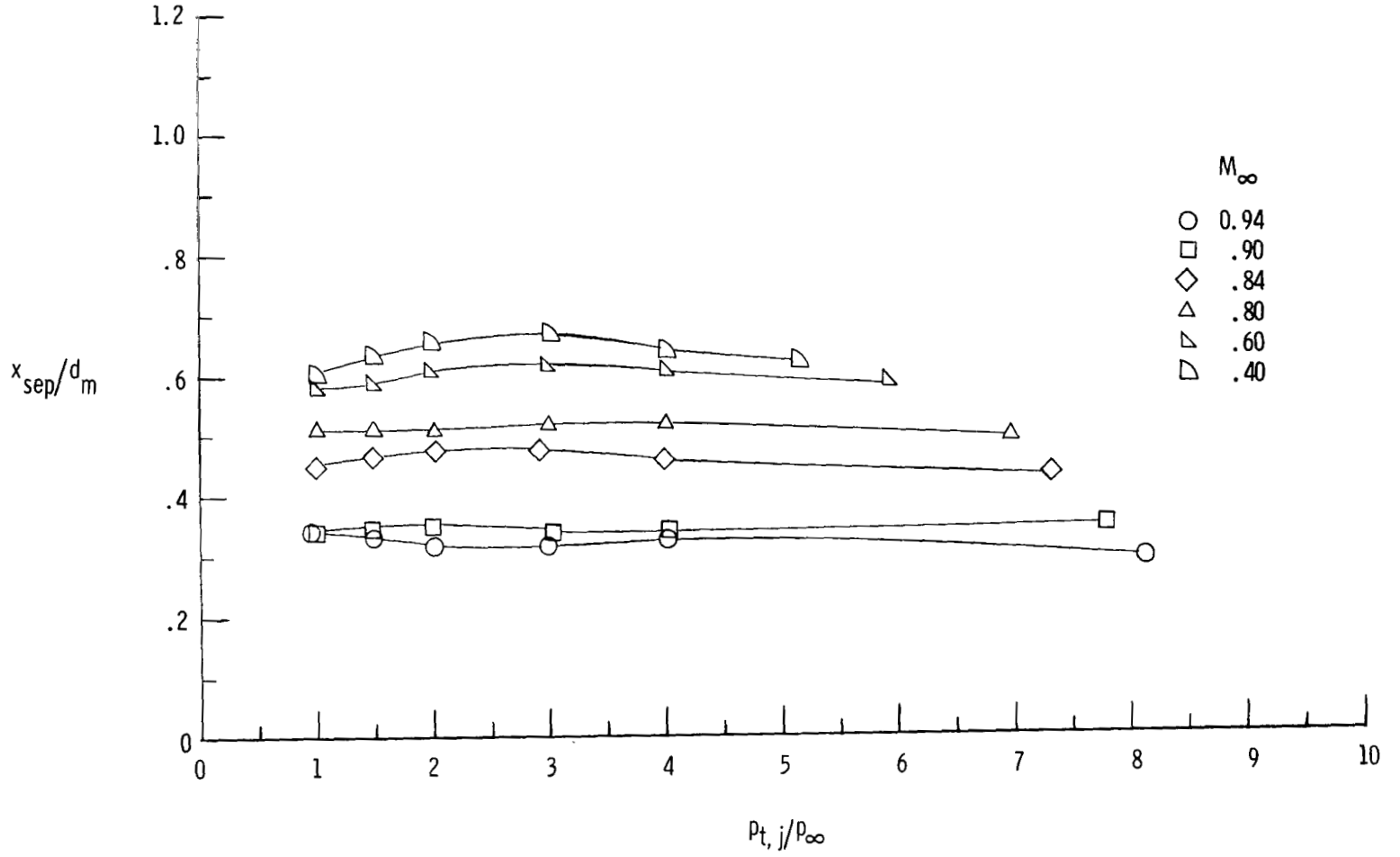

(a) Configuration 1 (l/d_m = 0.80; d_e/d_m = 0.50).

Figure 12.- Separation locations for configurations using high-pressure air to simulate jet exhausts.

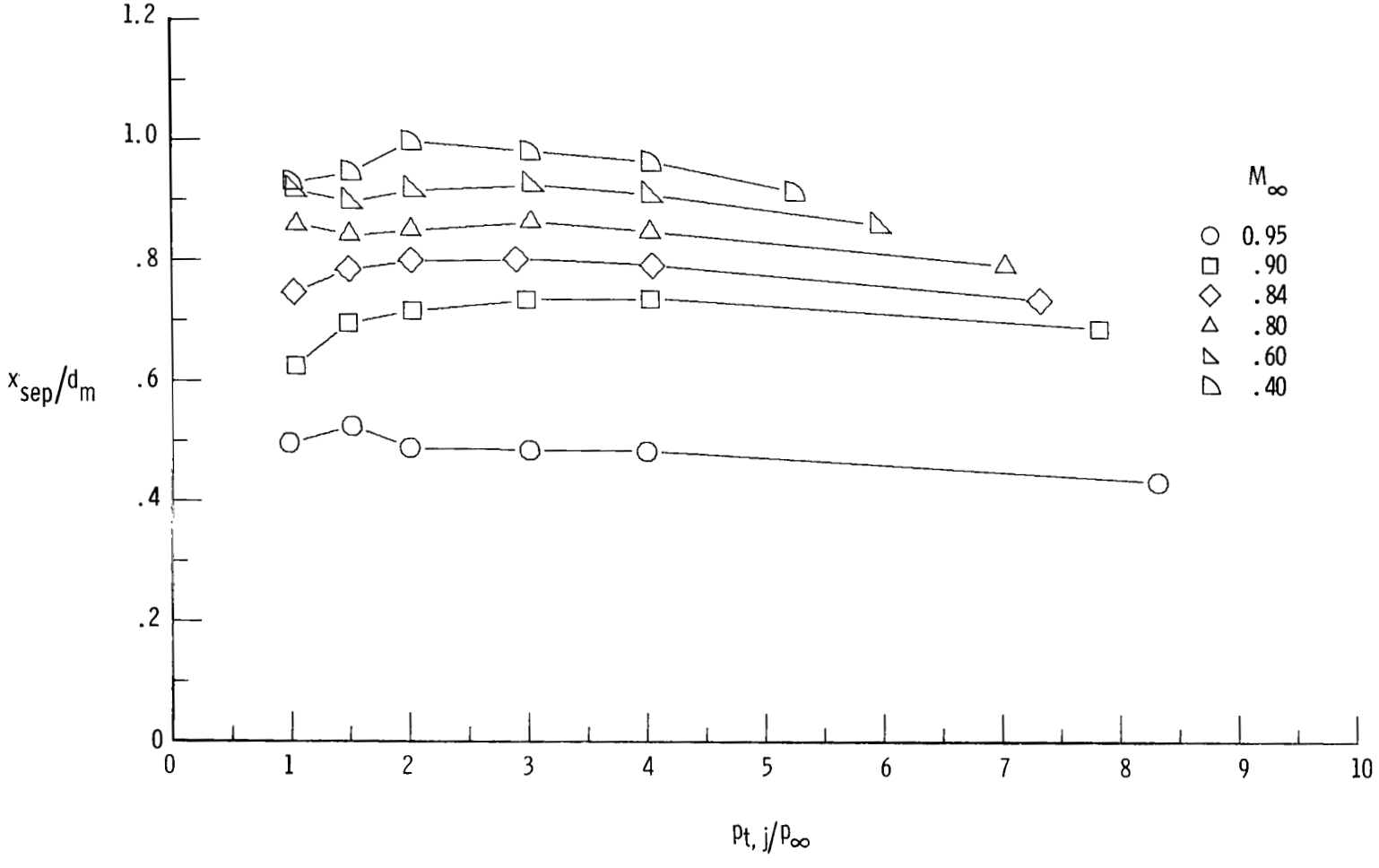

(b) Configuration 2 (ℓ/d_m = 1.00; d_e/d_m = 0.50).

Figure 12.- Continued.

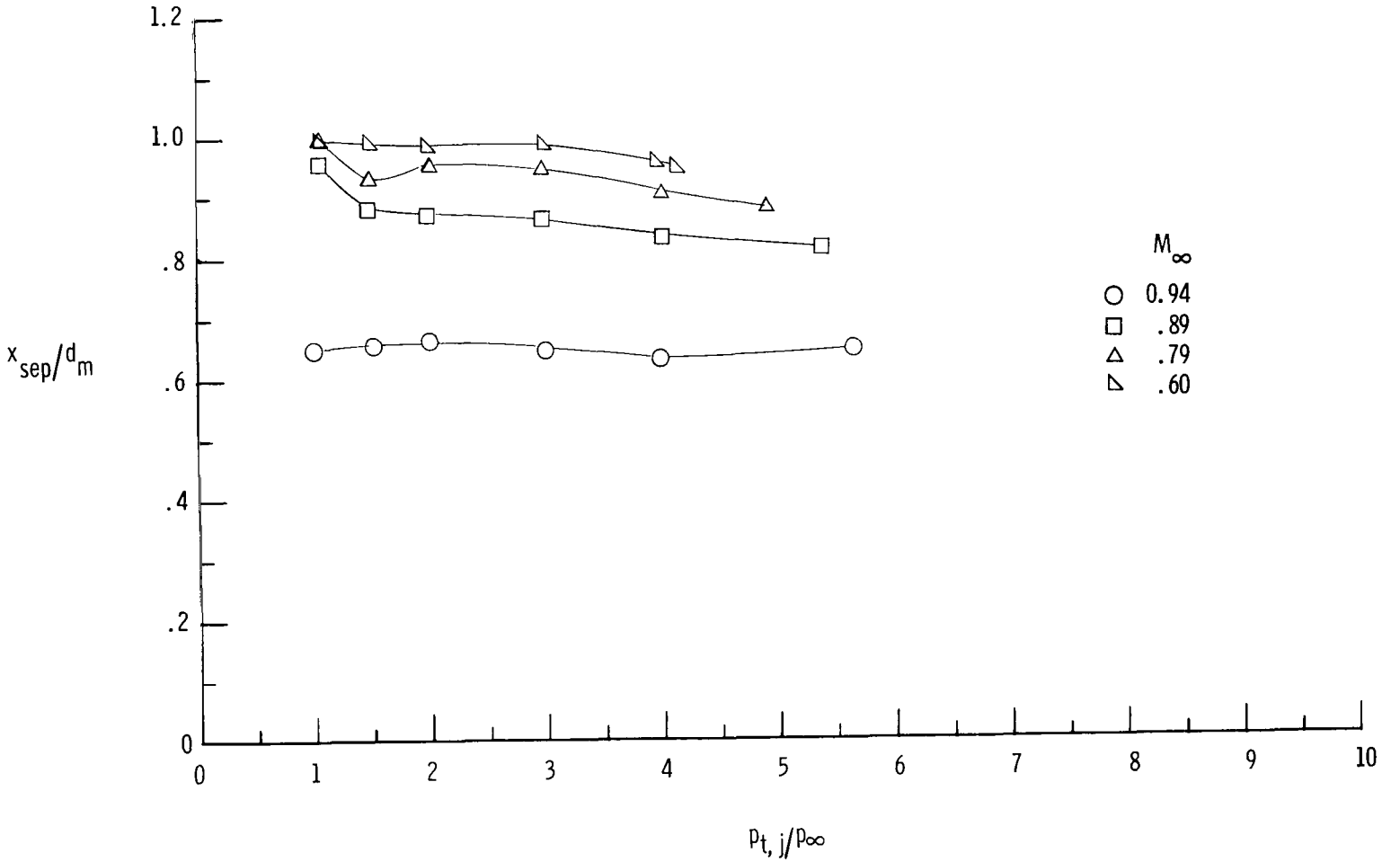

(c) Configuration 4 (l/d_m = 1.00; d_e/d_m = 0.60).

Figure 12.- Continued.

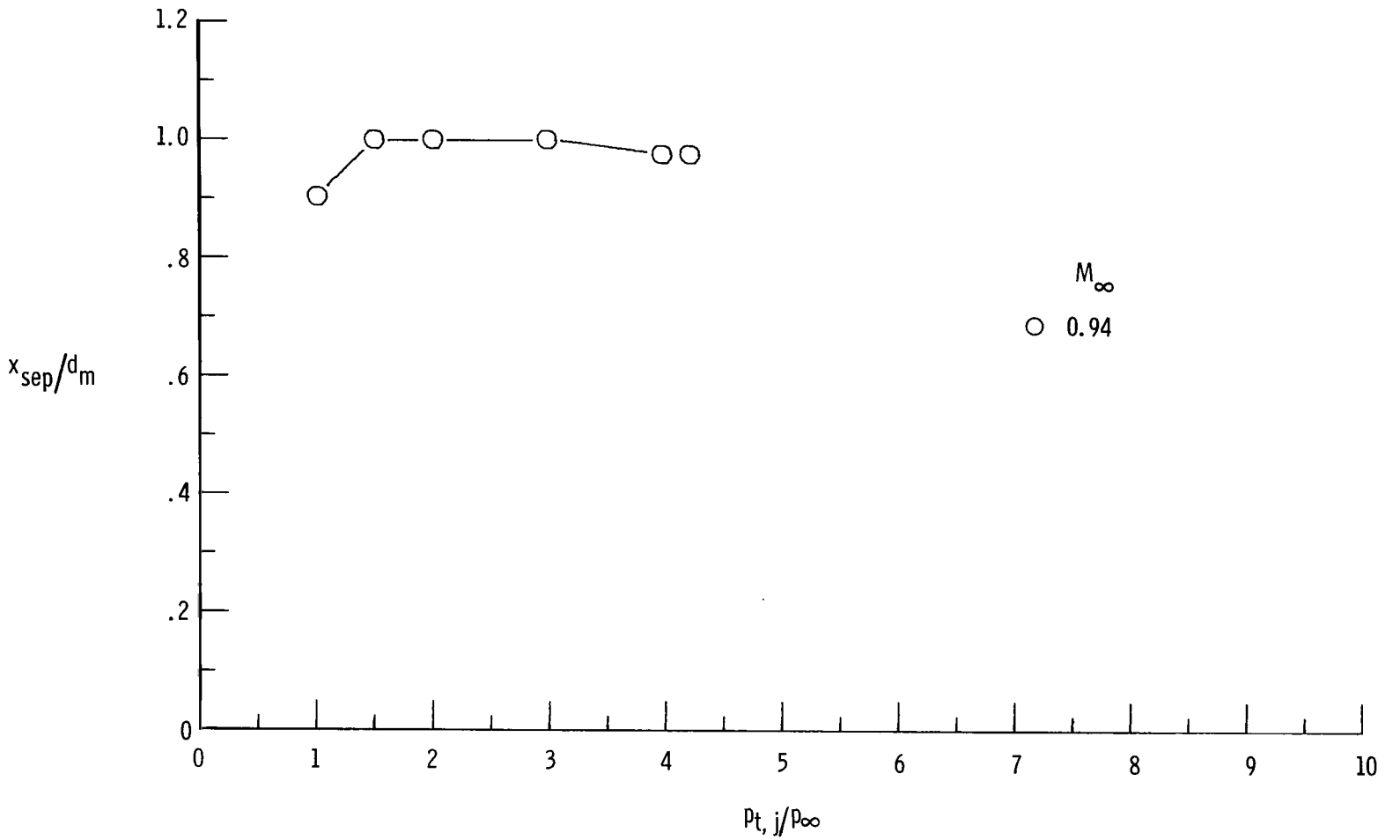

(d) Configuration 6 (l/d_m = 1.00; d_e/d_m = 0.70).

Figure 12.- Concluded.

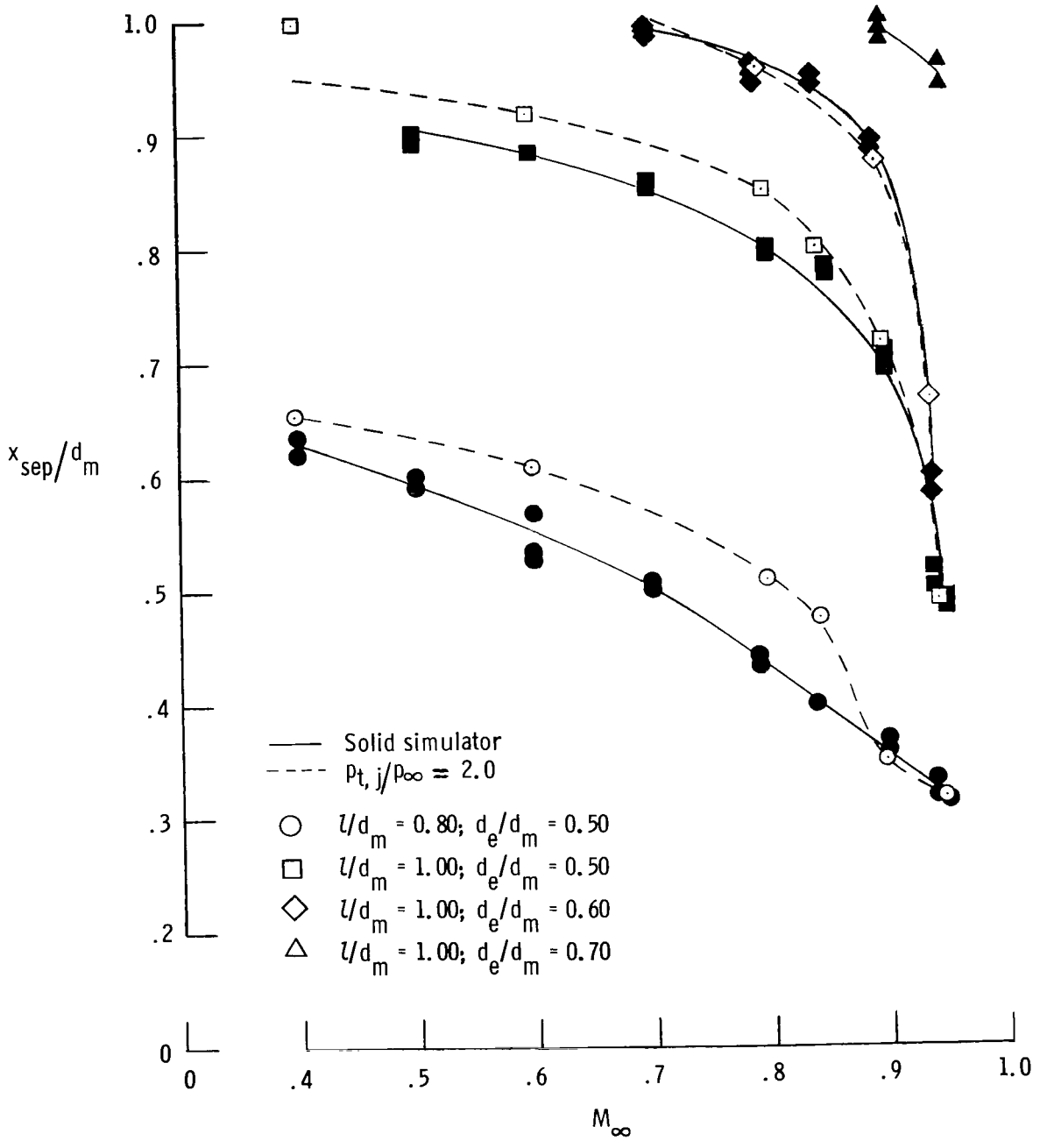

Figure 13.- Comparison between separation locations obtained through use of solid simulators (solid symbols) and separation locations obtained from jet operation at $p_{t,j}/p_\infty = 2.00$ (open symbols).

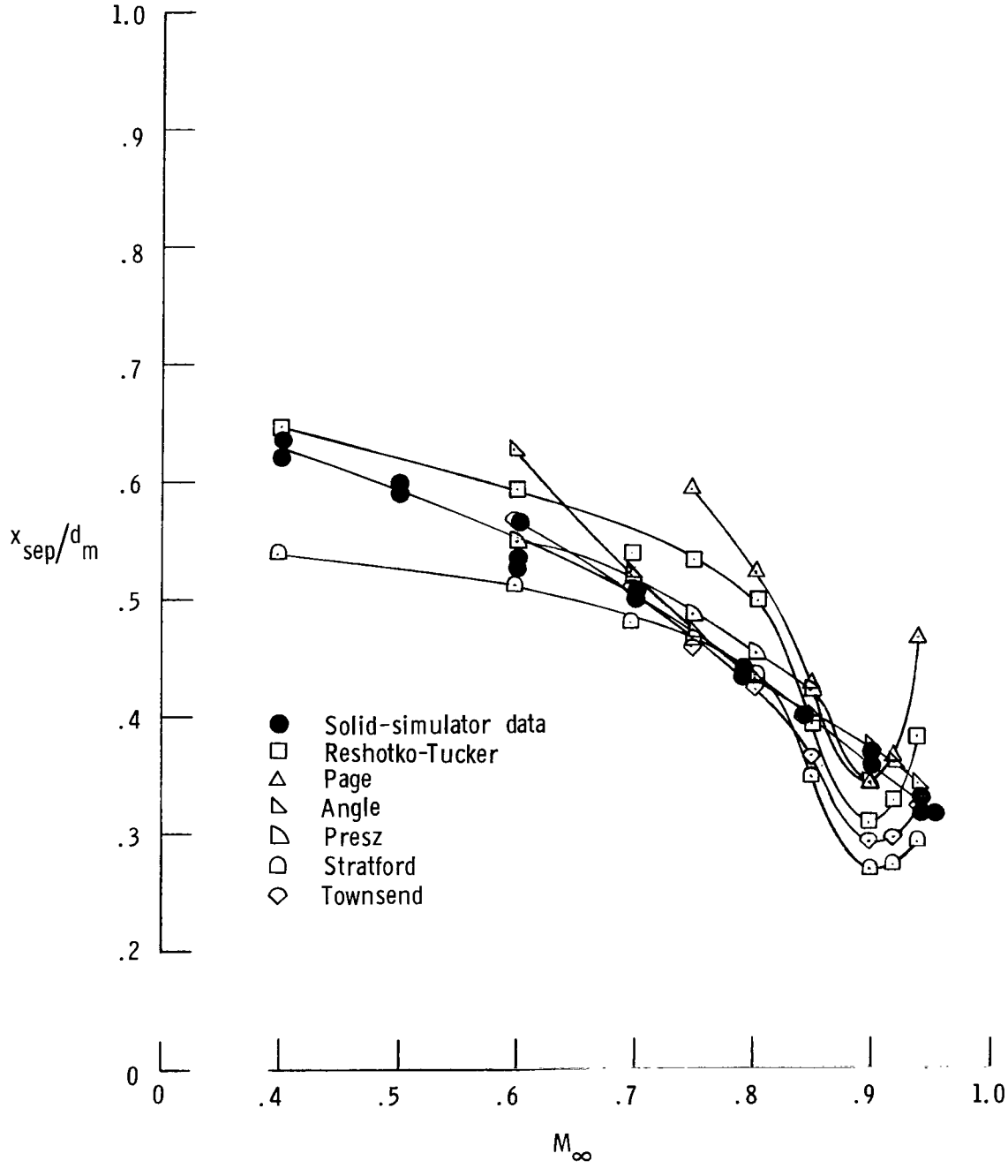

(a) Configuration 1 (l/d_m = 0.80; d_e/d_m = 0.50).

Figure 14.- Variation with Mach number of solid-simulator separation data and predicted separation locations based on experimental pressure distributions.

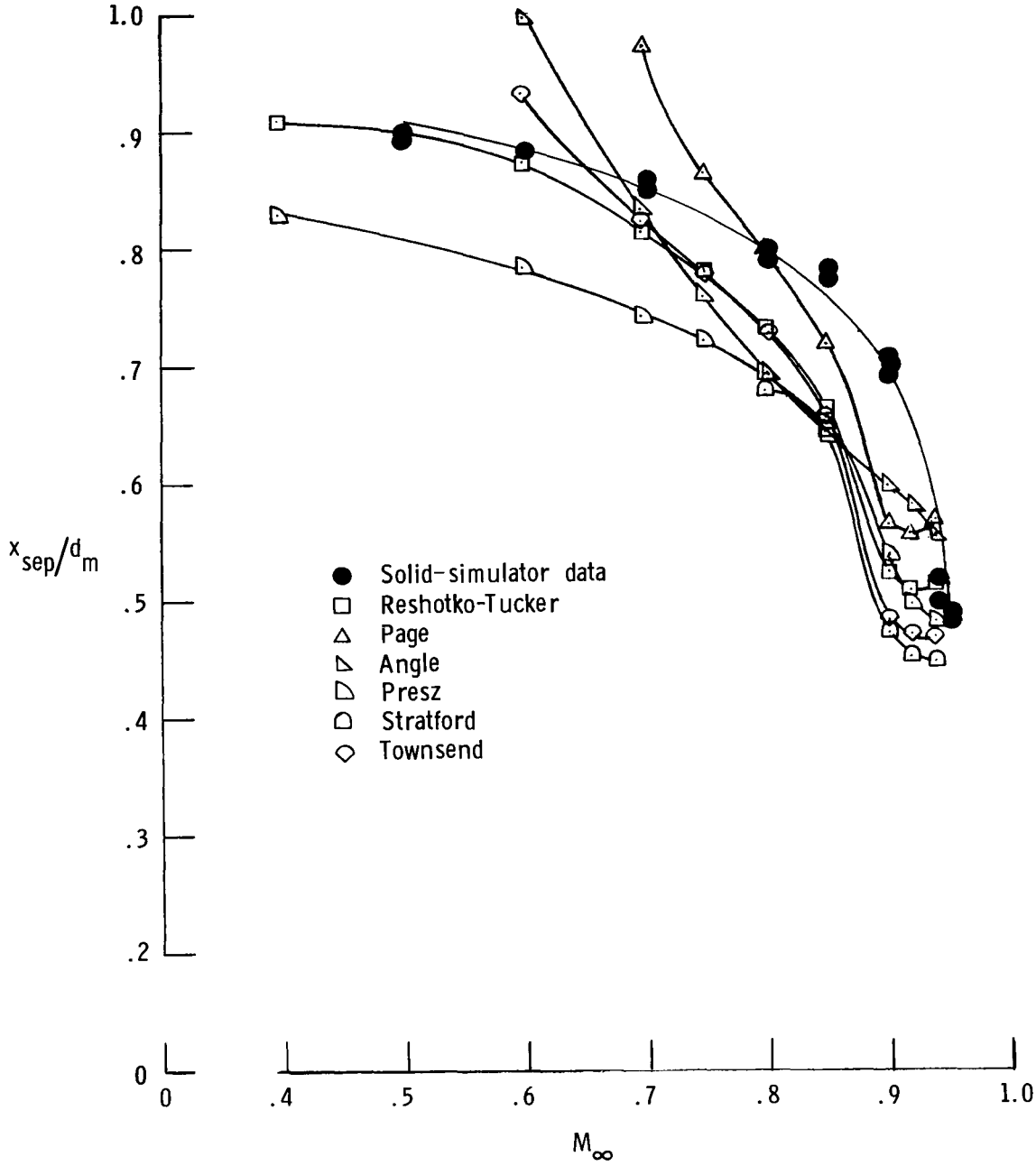

(b) Configuration 2 (l/d_m = 1.00; d_e/d_m = 0.50).

Figure 14.- Continued.

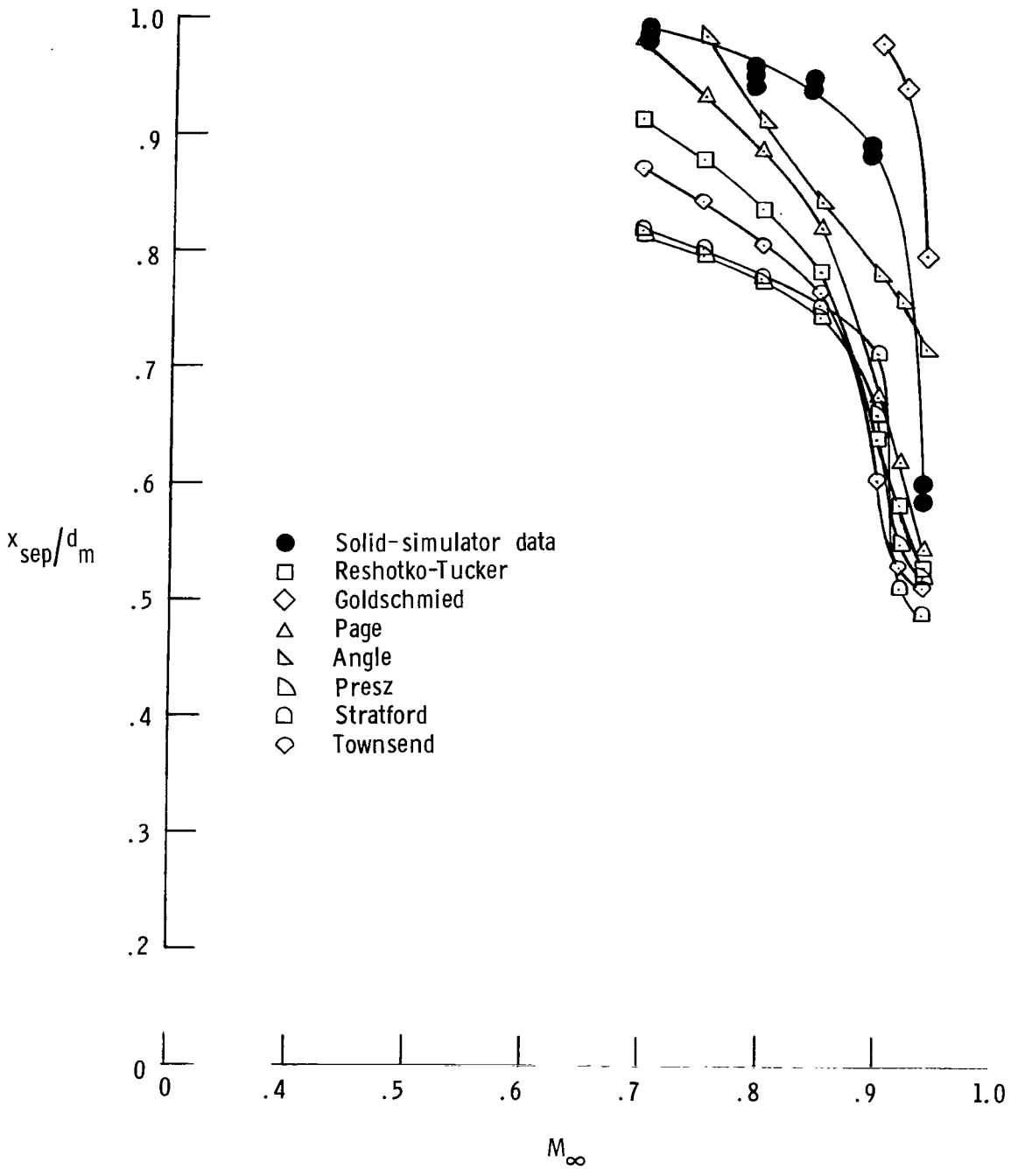

(c) Configuration 4 (l/d_m = 1.00; d_e/d_m = 0.60).

Figure 14.- Continued.

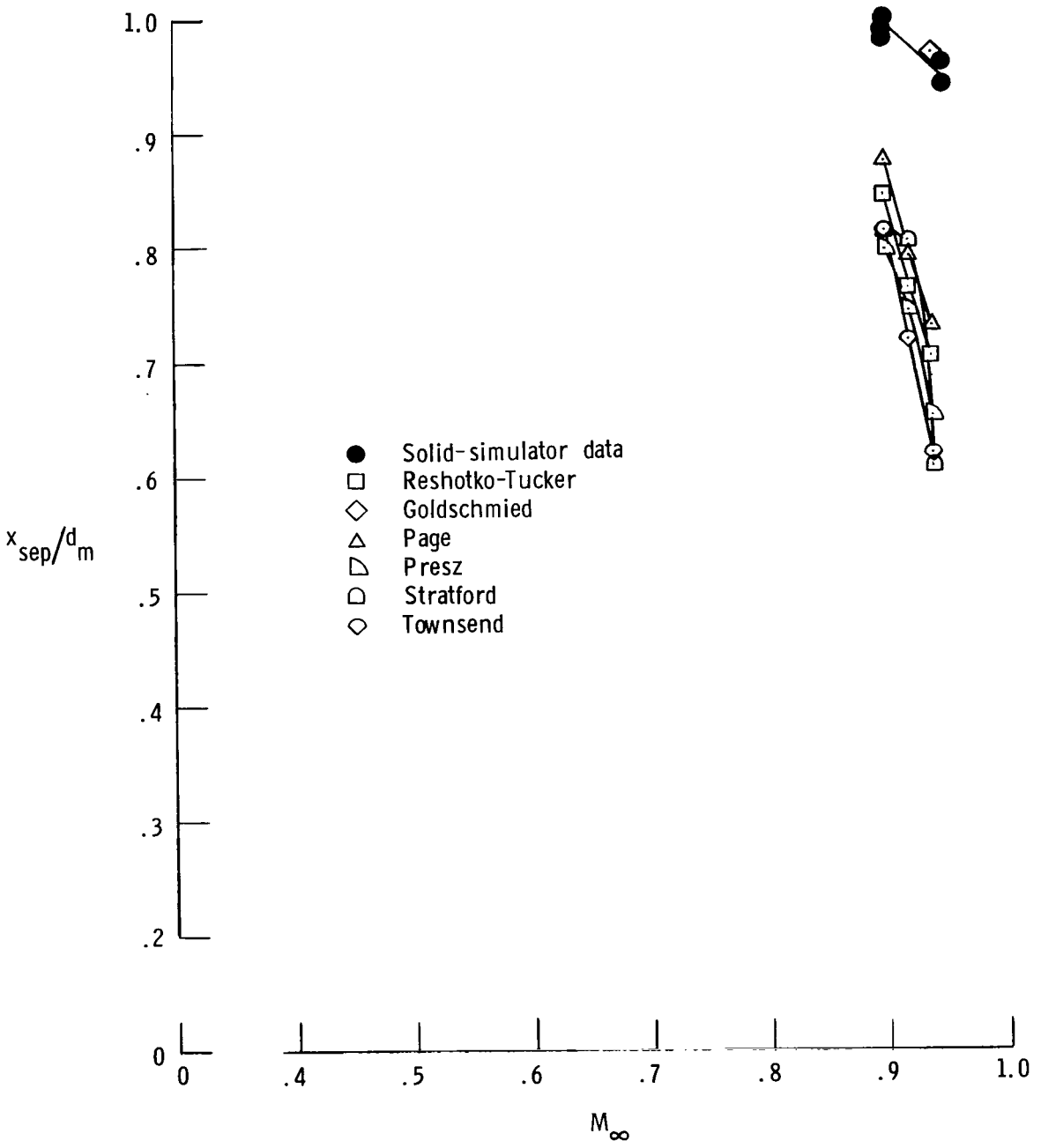

(d) Configuration 6 (l/d_m = 1.00; d_e/d_m = 0.70).

Figure 14.- Concluded.

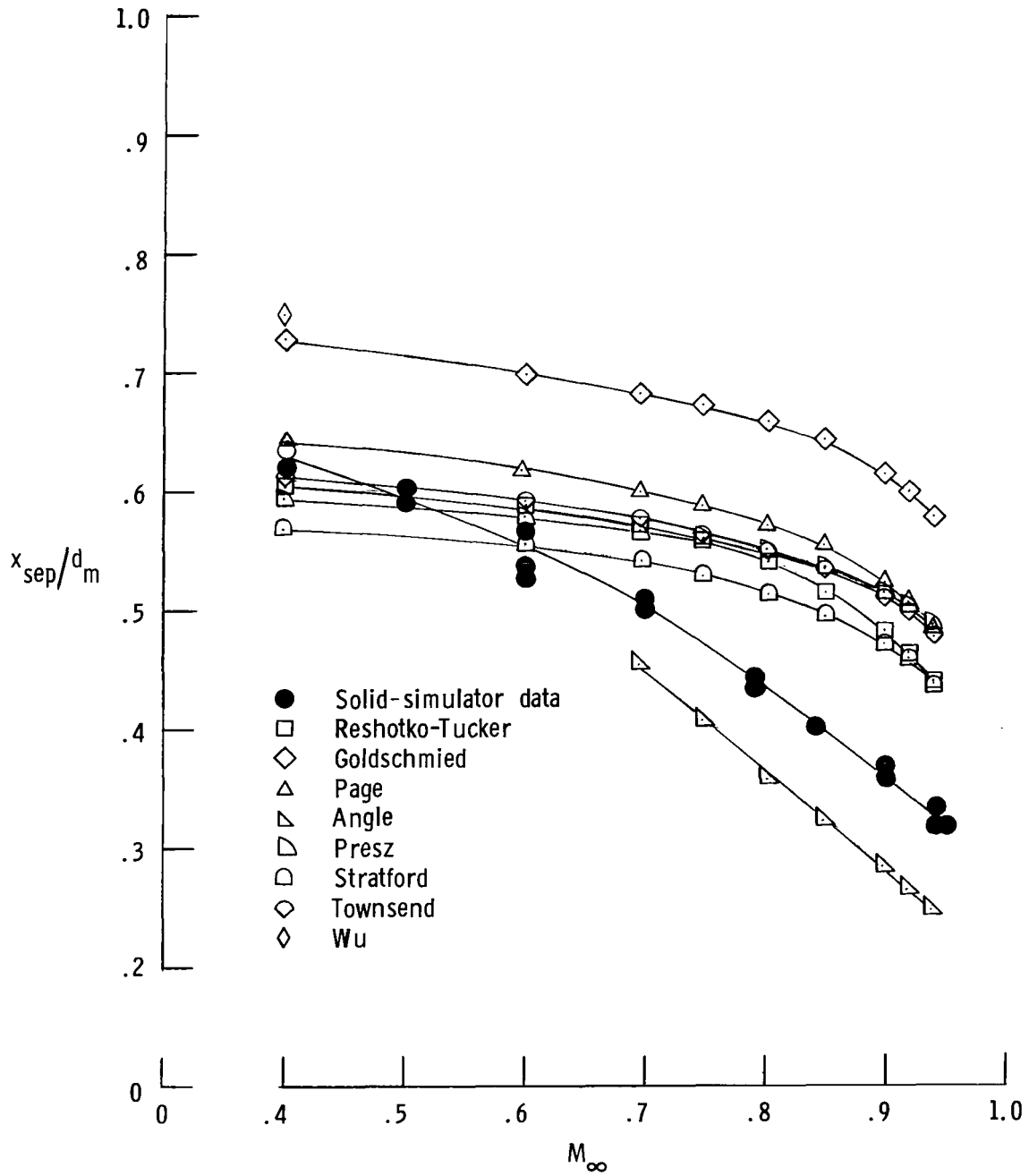

(a) Configuration 1 (l/d_m = 0.80; d_e/d_m = 0.50).

Figure 15.- Variation with Mach number of solid-simulator separation data and predicted separation locations based on theoretical inviscid pressure distributions.

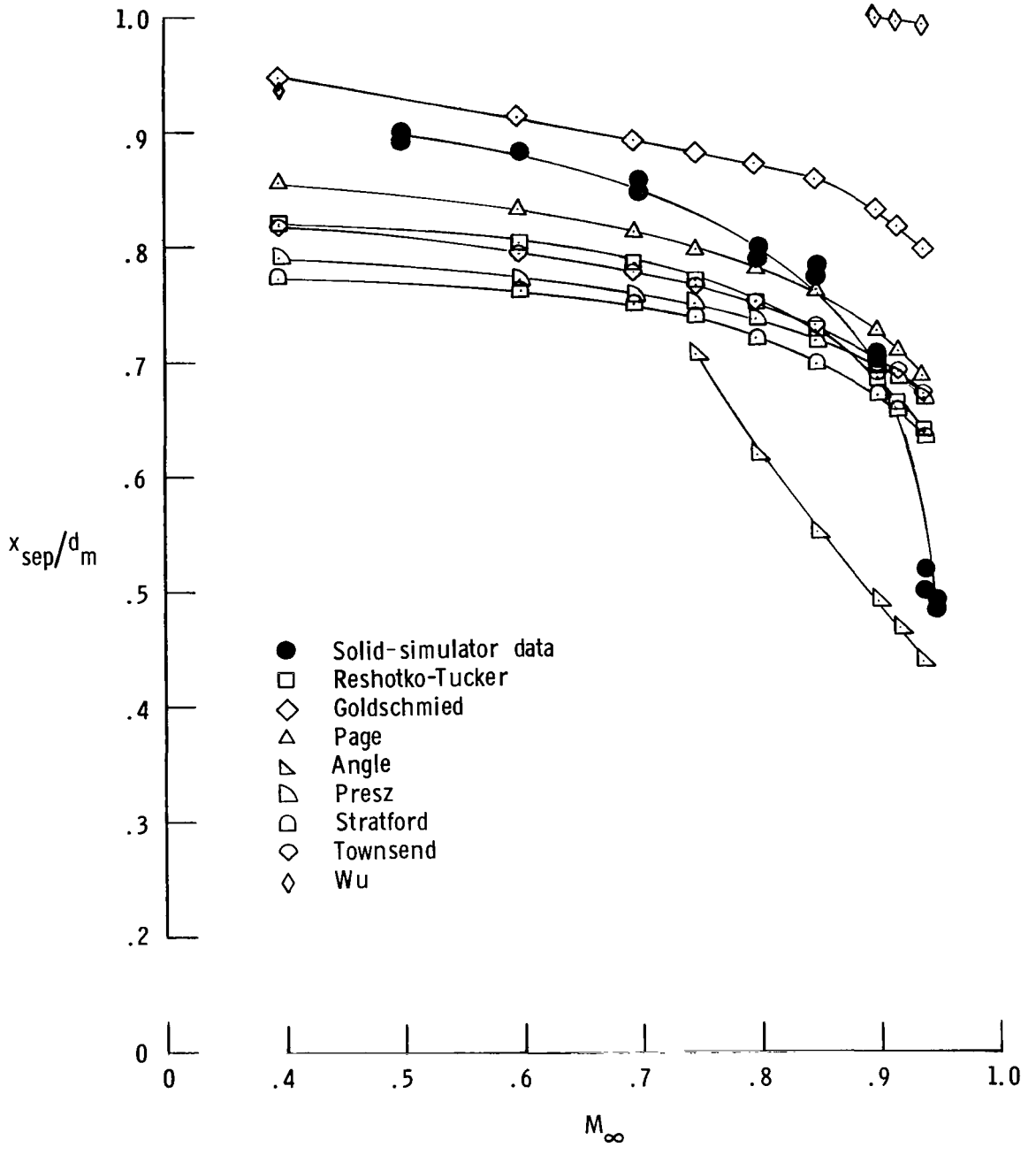

(b) Configuration 2 (l/d_m = 1.00; d_e/d_m = 0.50).

Figure 15.- Continued.

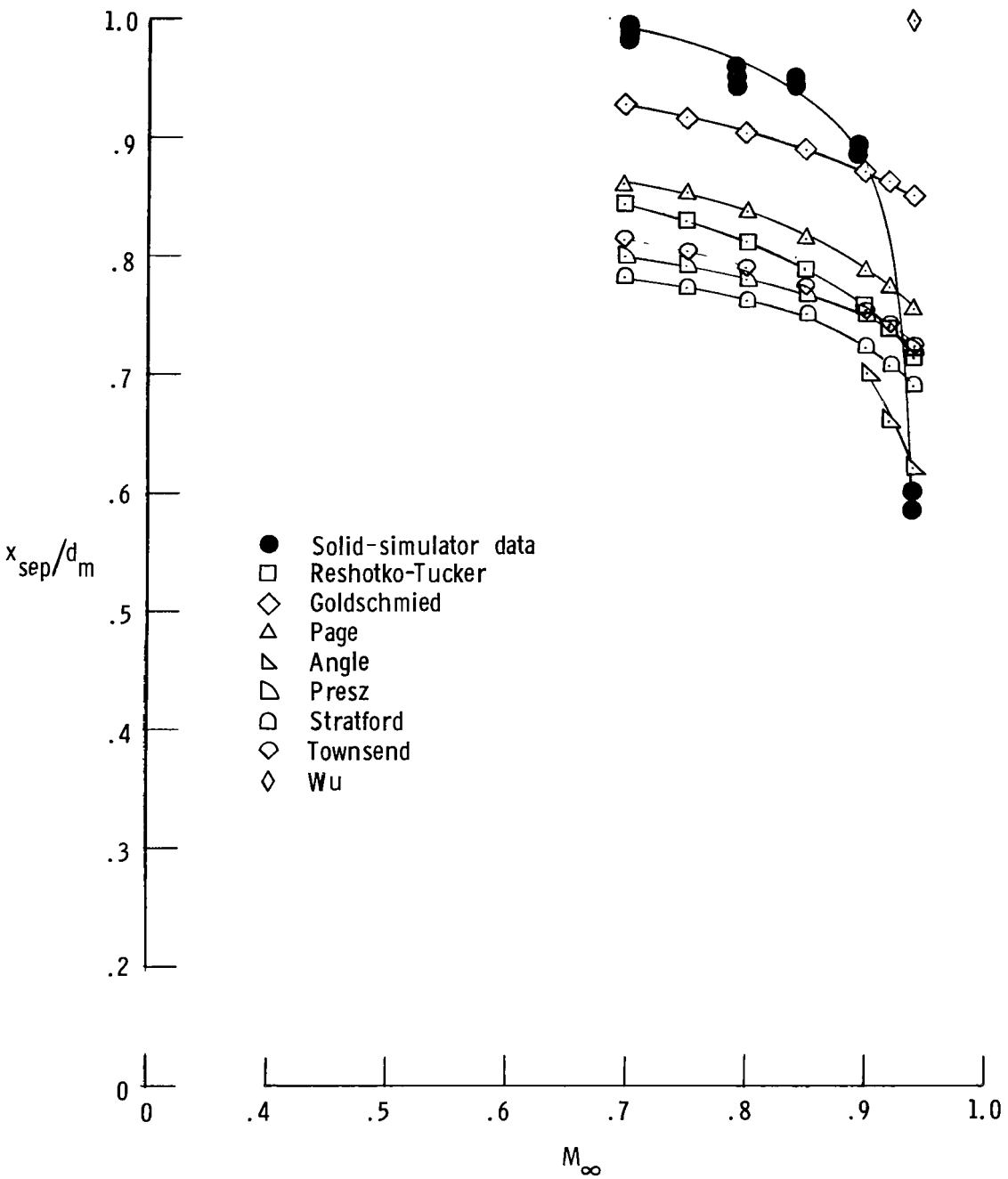

(c) Configuration 4 (l/d_m = 1.00; d_e/d_m = 0.60).

Figure 15.- Continued.

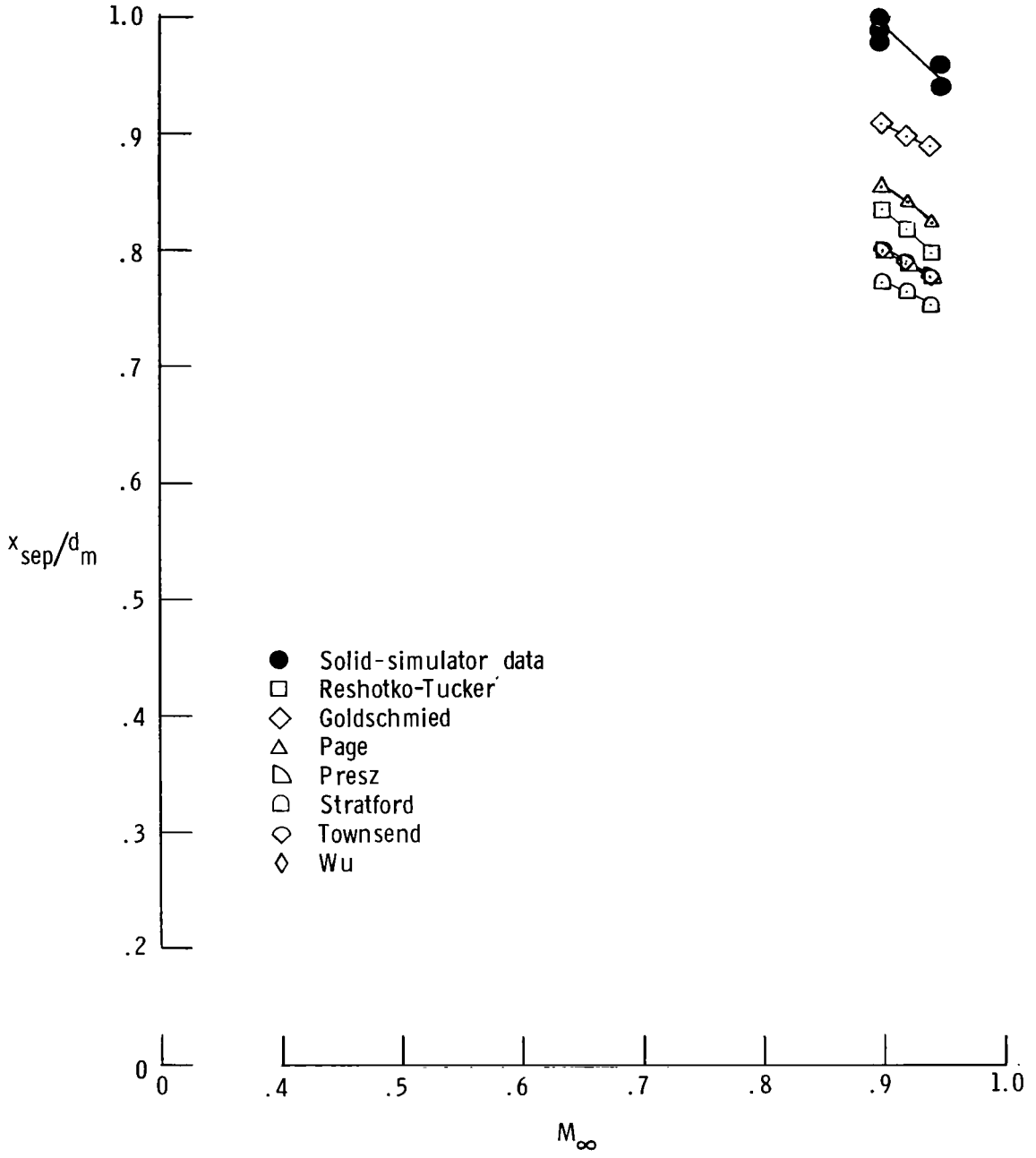

(d) Configuration 6 (l/d_m = 1.00; d_e/d_m = 0.70).

Figure 15.- Concluded.

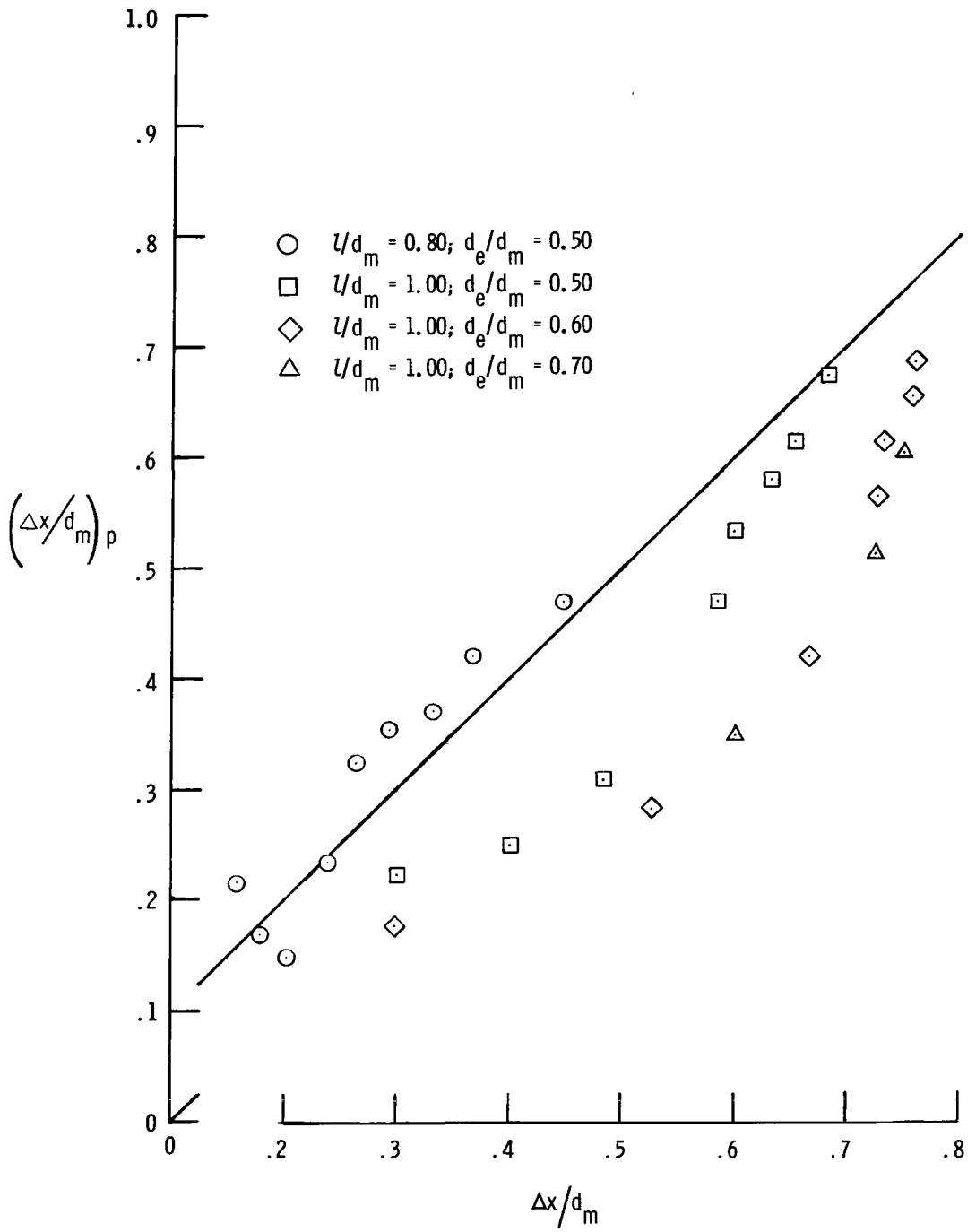

(a) Reshotko-Tucker.

Figure 16.- Predicted separation locations based on experimental pressure distributions as function of solid-simulator separation data.

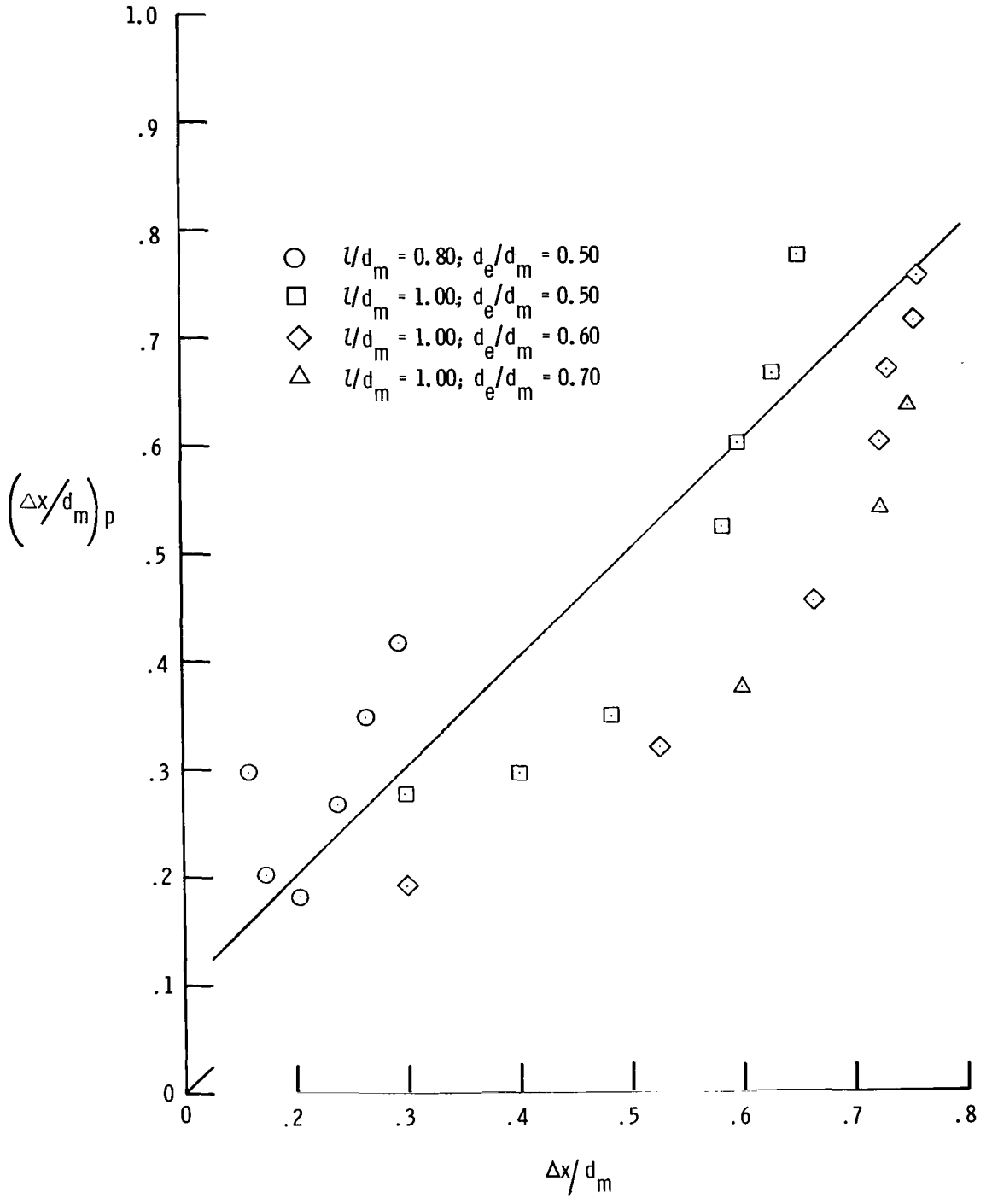

(b) Page.

Figure 16.- Continued.

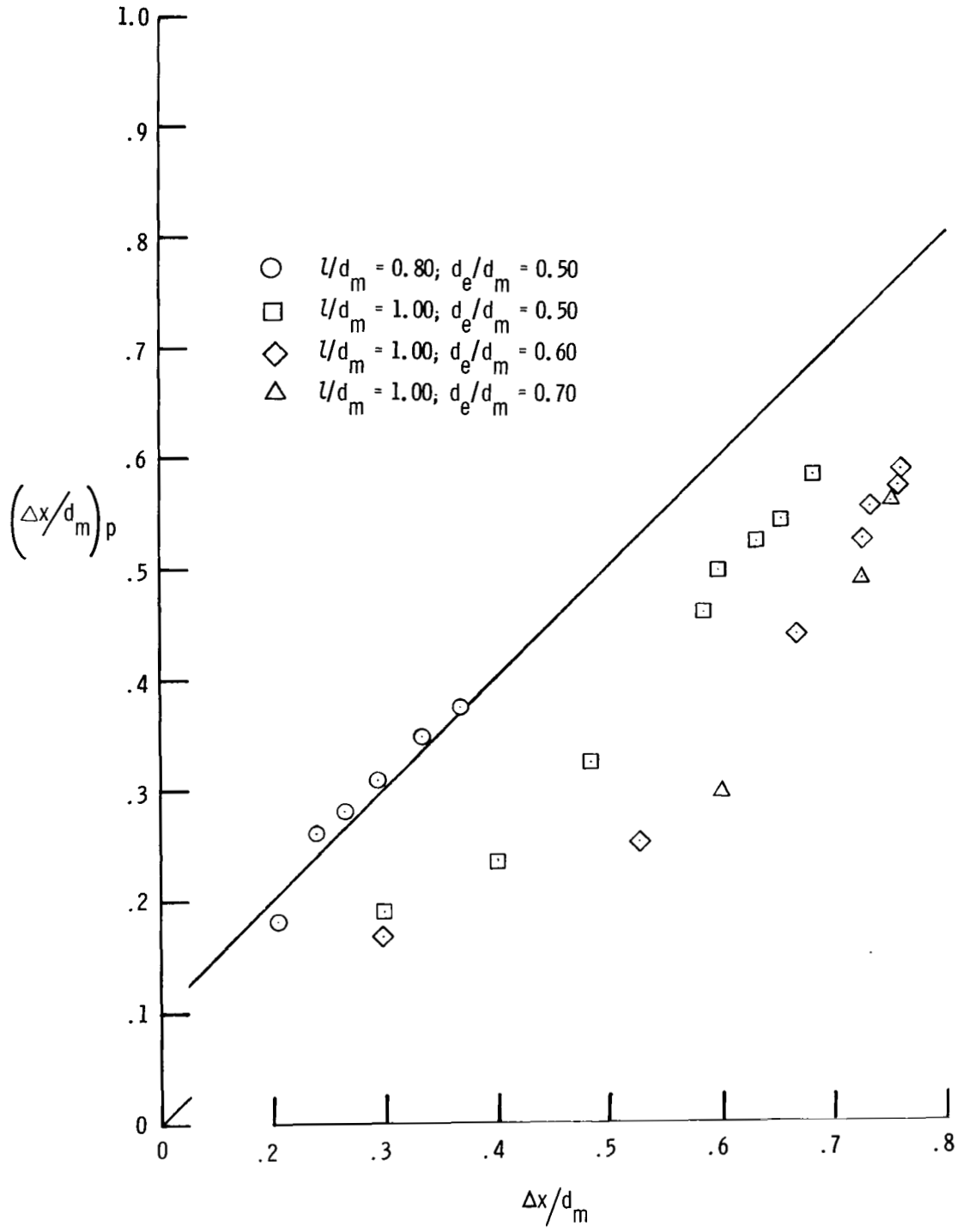

(c) Presz.

Figure 16.- Continued.

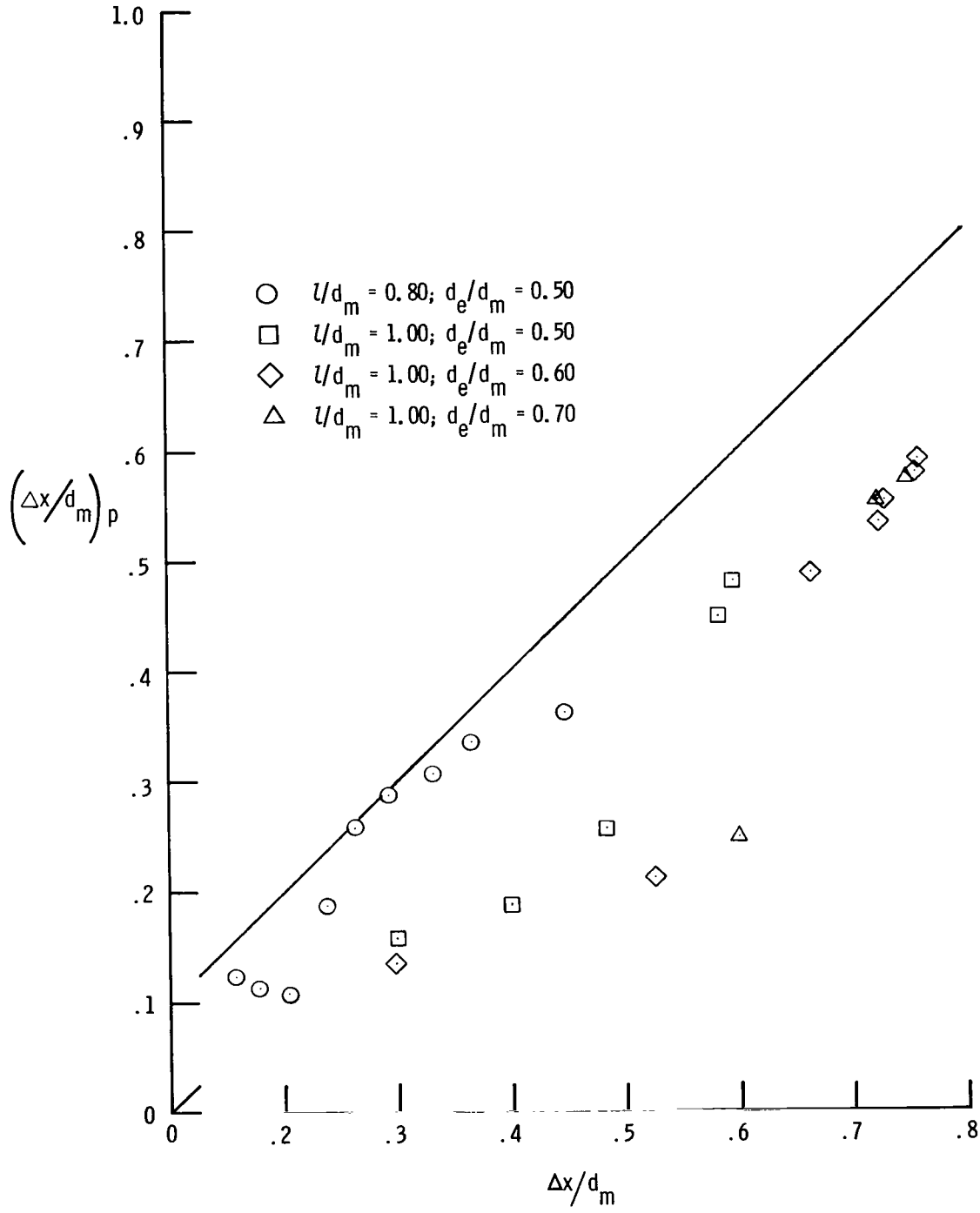

(d) Stratford.

Figure 16.- Continued.

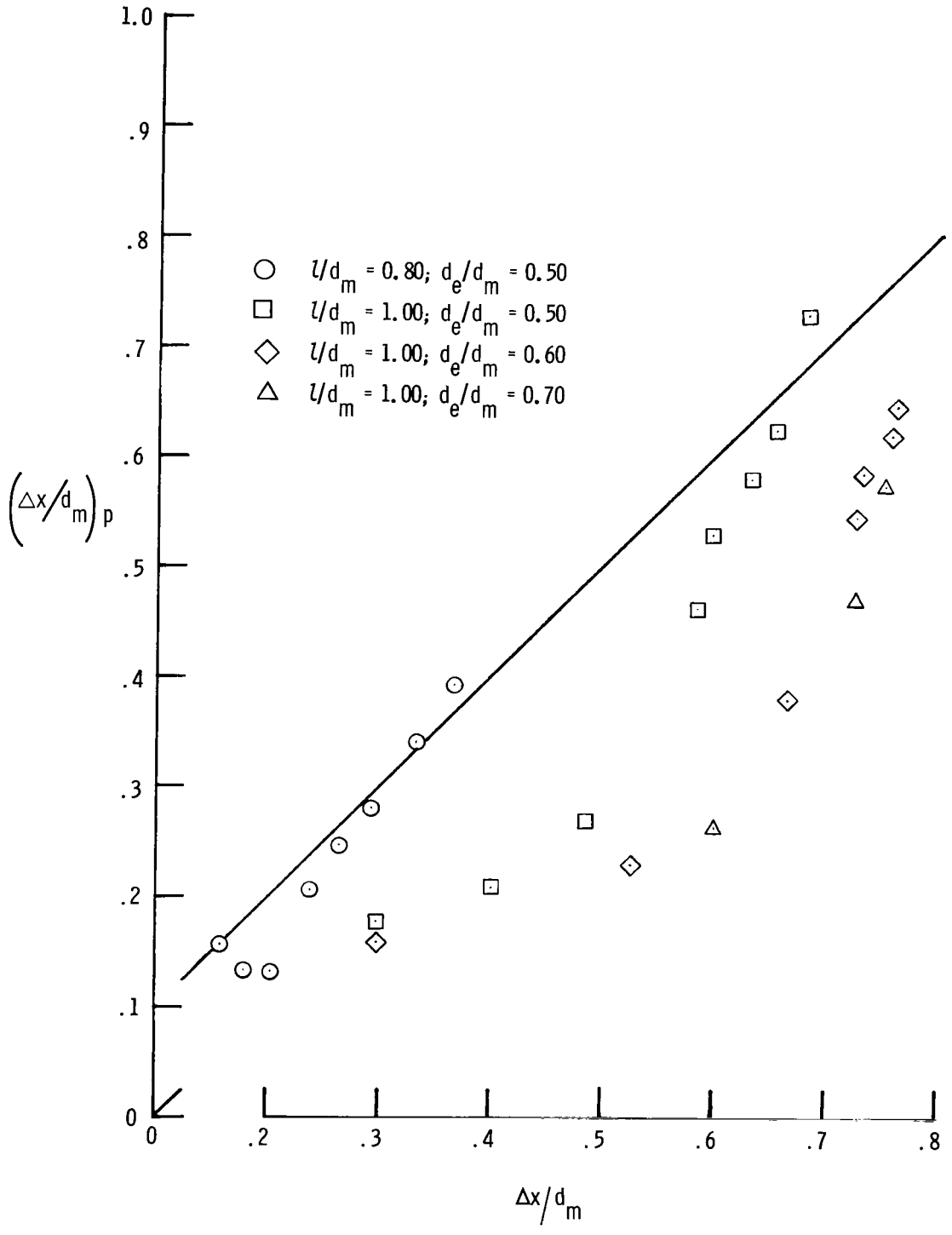

(e) Townsend.

Figure 16.- Continued.

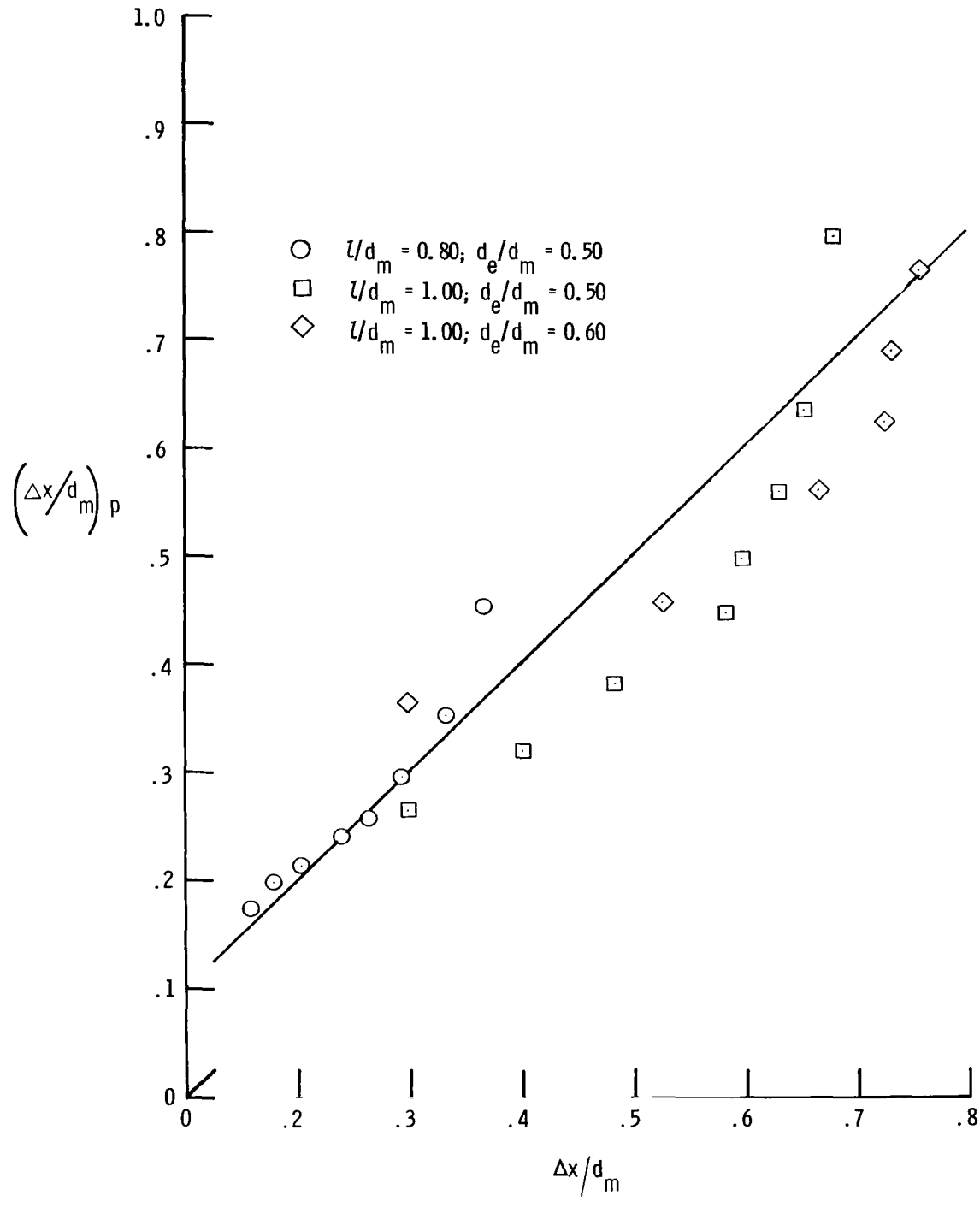

(f) Angle.

Figure 16.- Concluded.

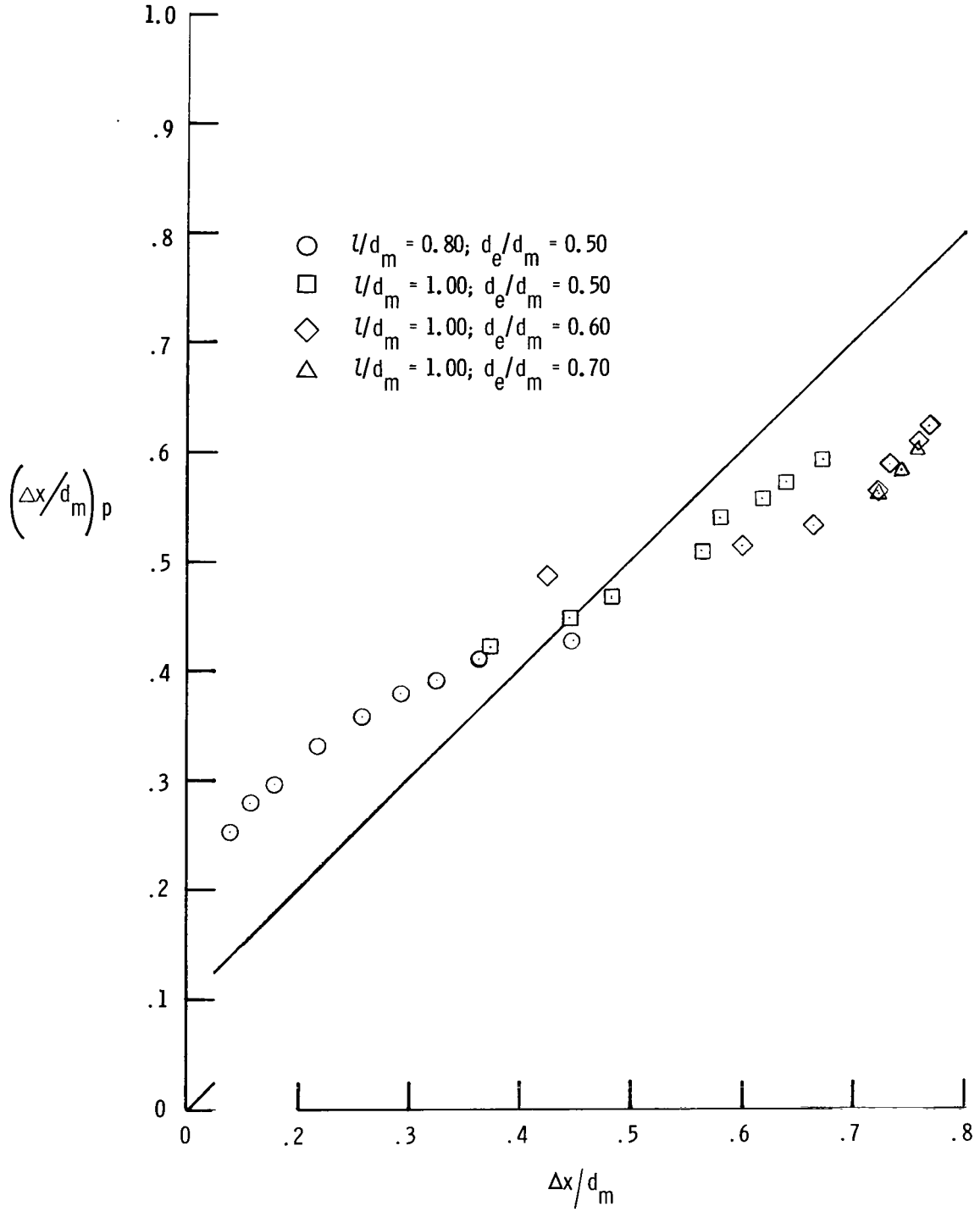

(a) Reshotko-Tucker.

Figure 17.- Predicted separation locations based on theoretical inviscid pressure distributions as function of solid-simulator separation data.

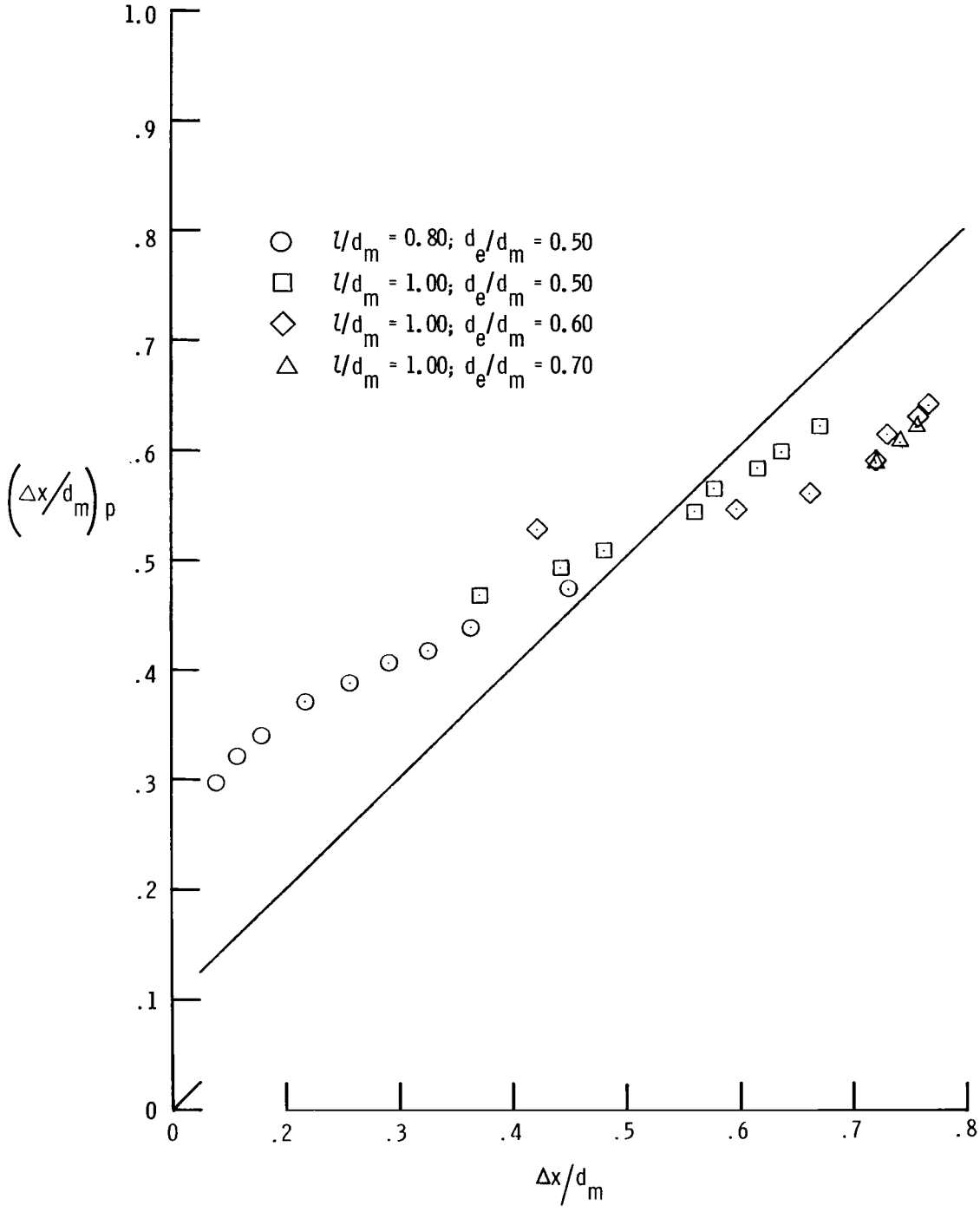

(b) Page.

Figure 17.- Continued.

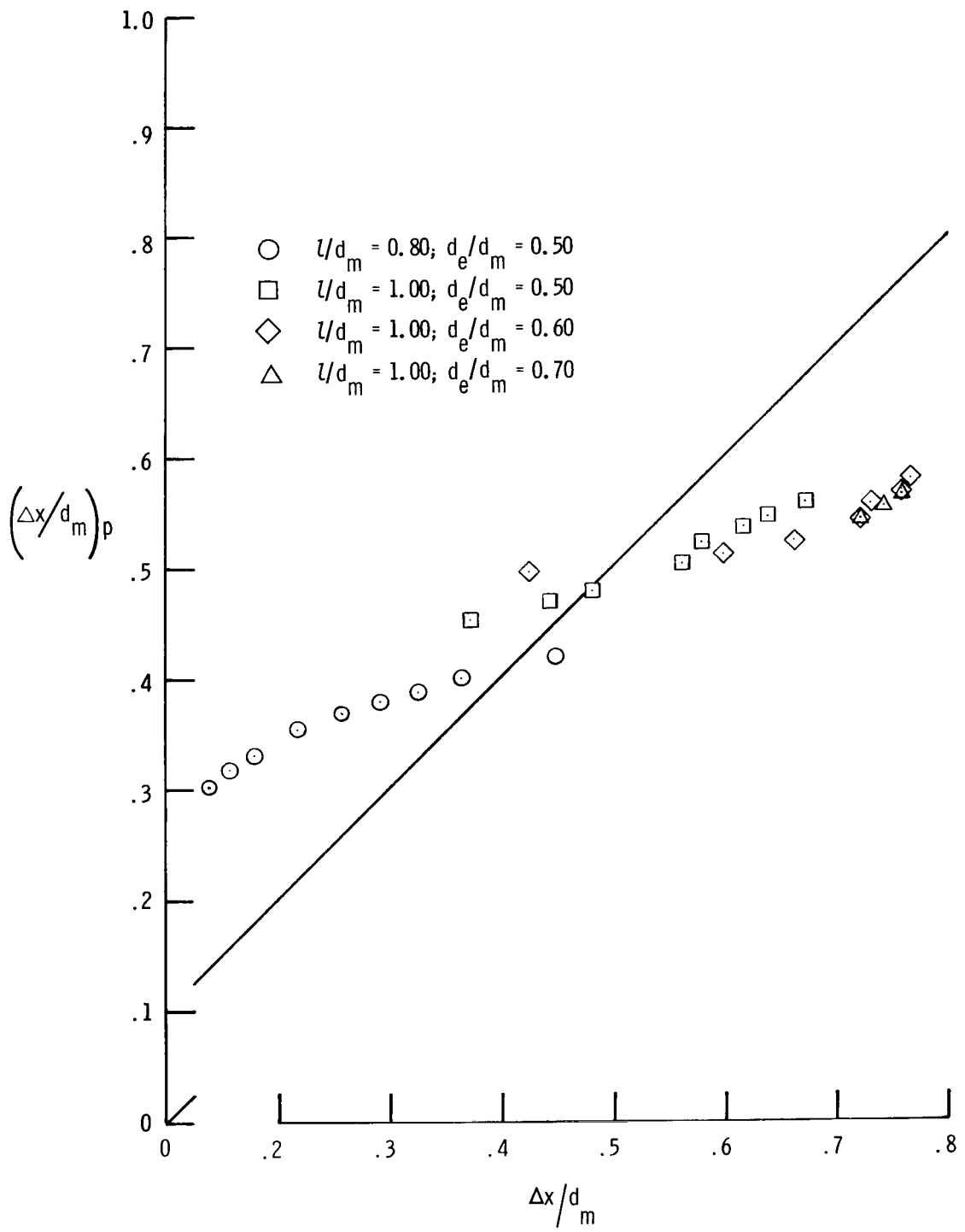

(c) Presz.

Figure 17.- Continued.

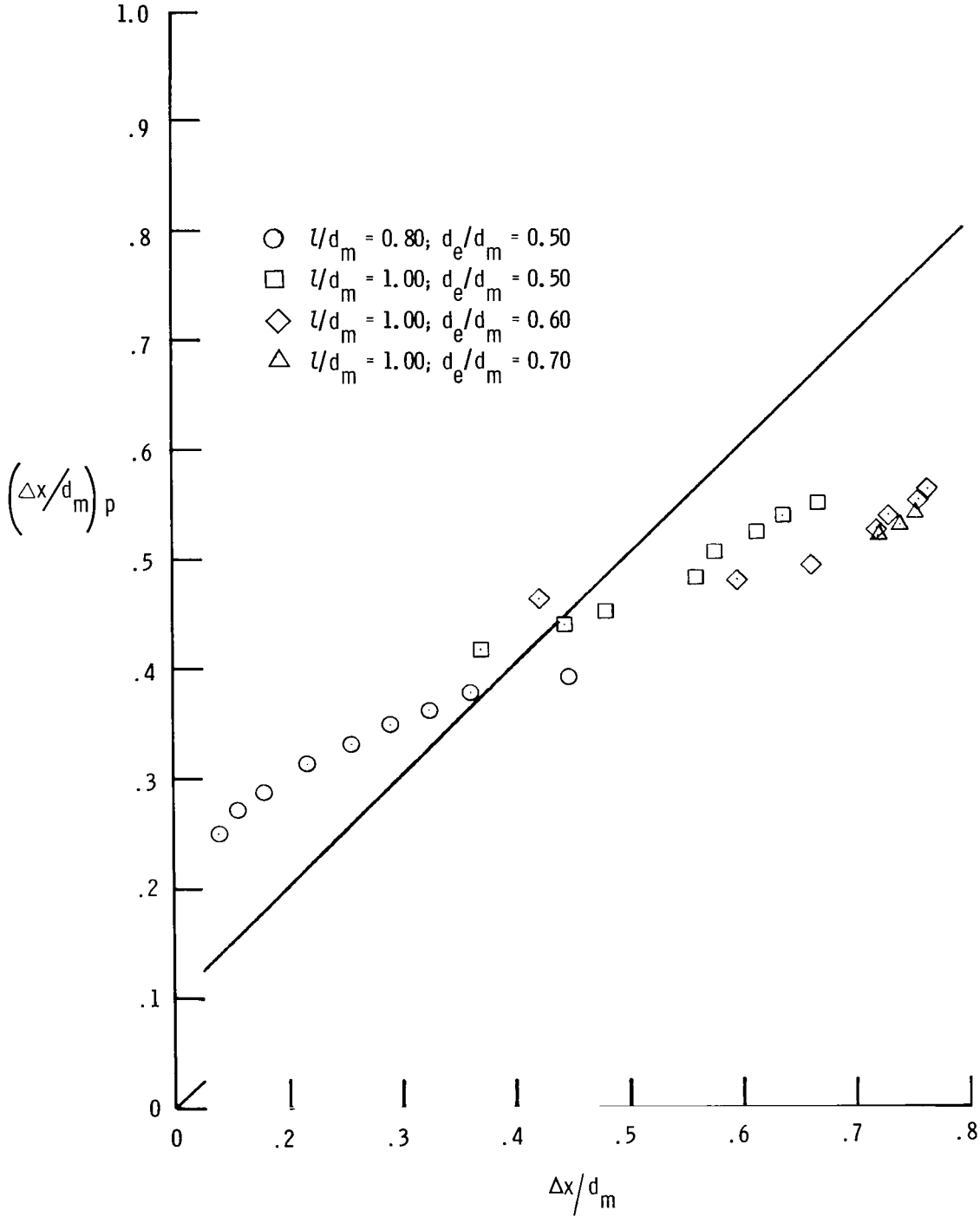

(d) Stratford.

Figure 17.- Continued.

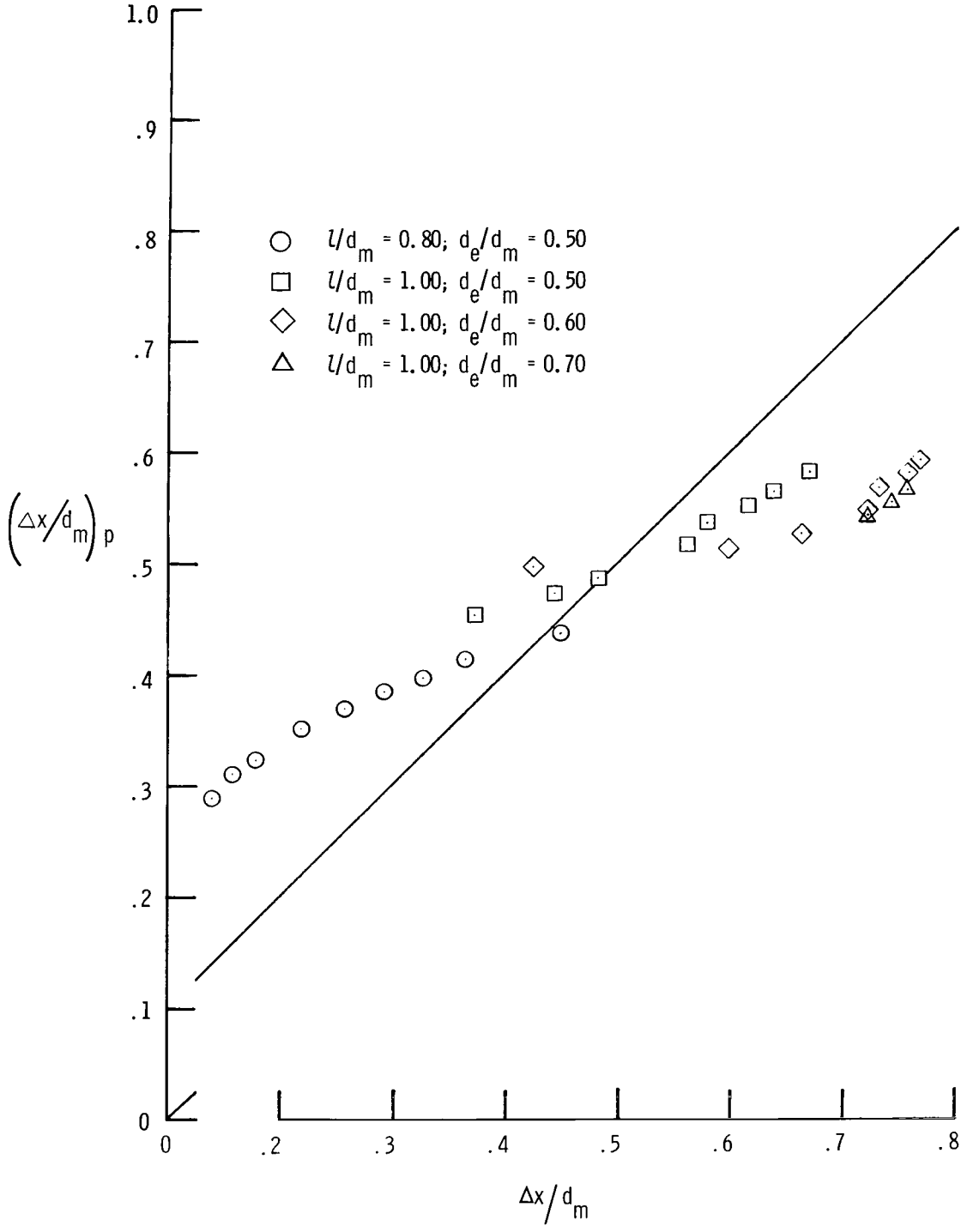

(e) Townsend.

Figure 17.- Continued.

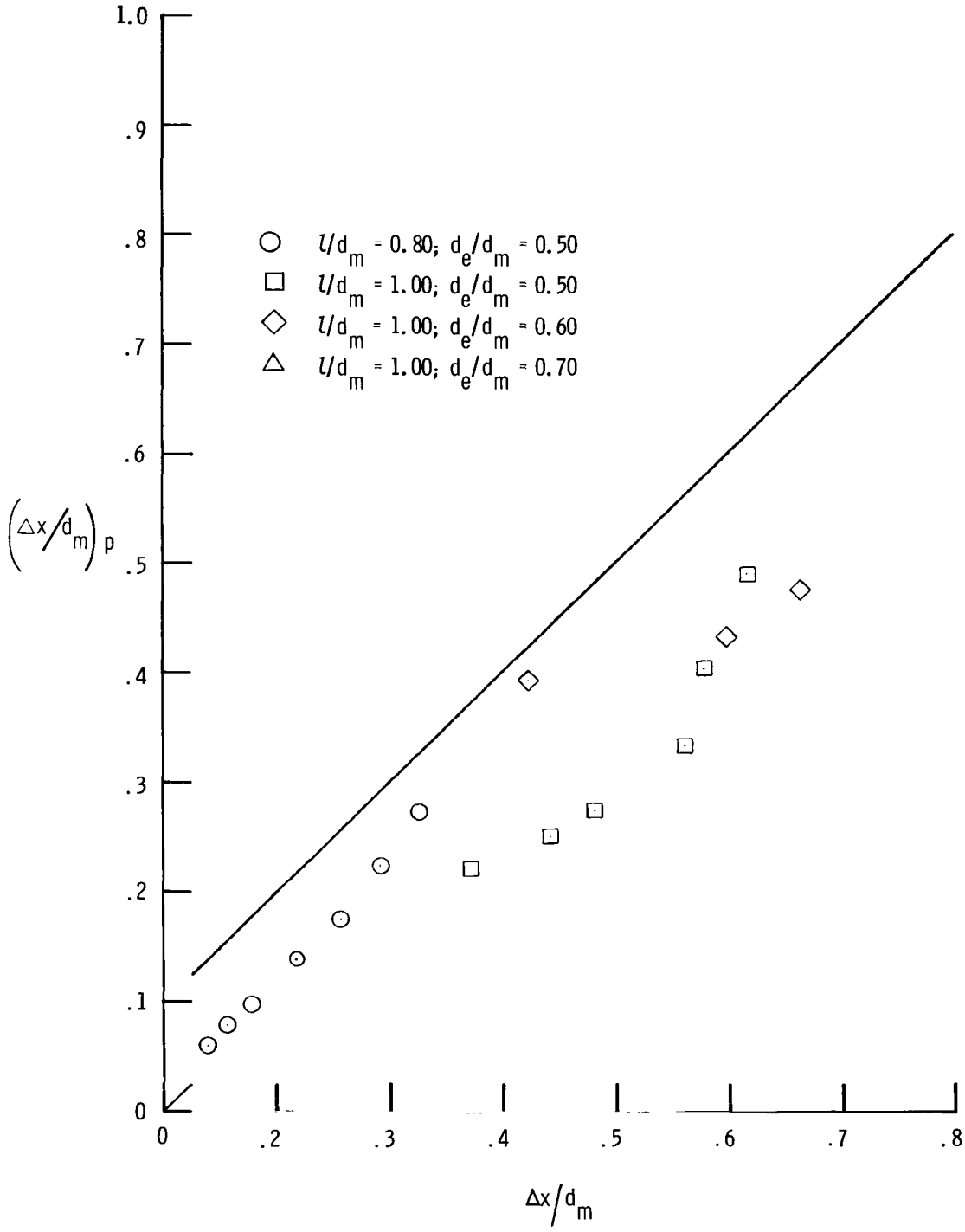

(f) Angle.

Figure 17.- Continued.

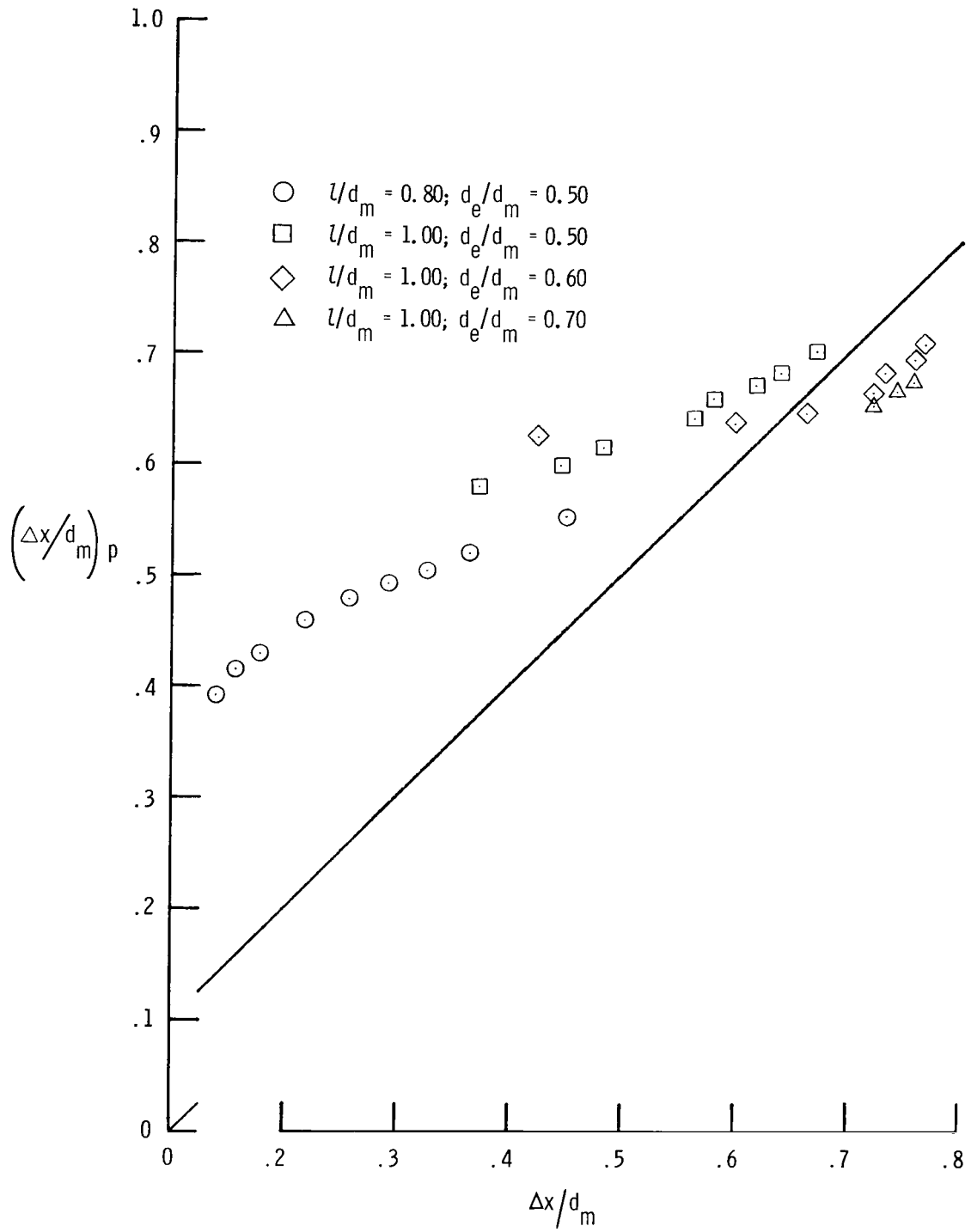

(g) Goldschmied.

Figure 17.- Concluded.

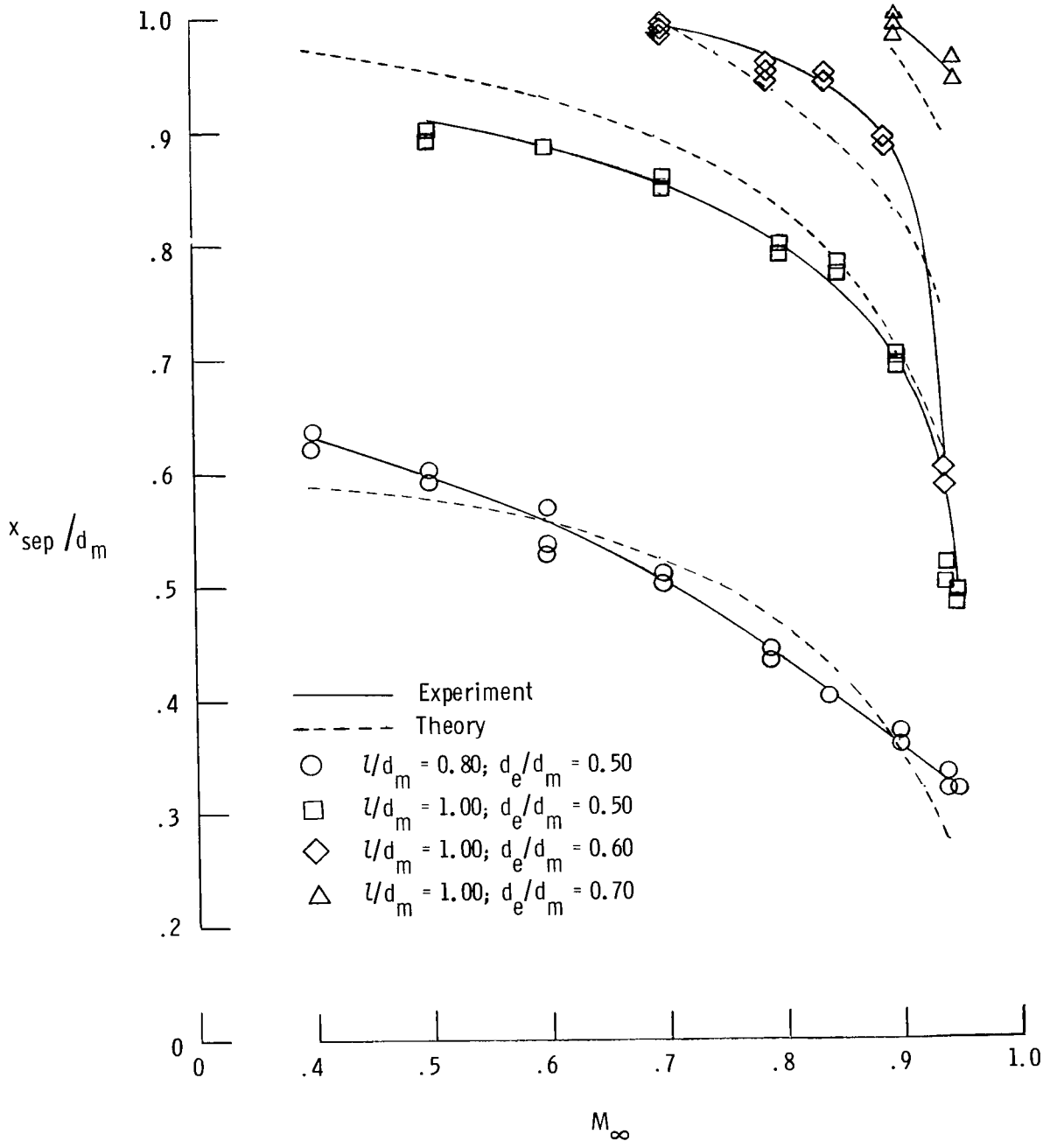

Figure 18.- Comparison of solid-simulator separation data and predicted separation locations made by applying least-squares curve fit to Reshotko-Tucker criterion.

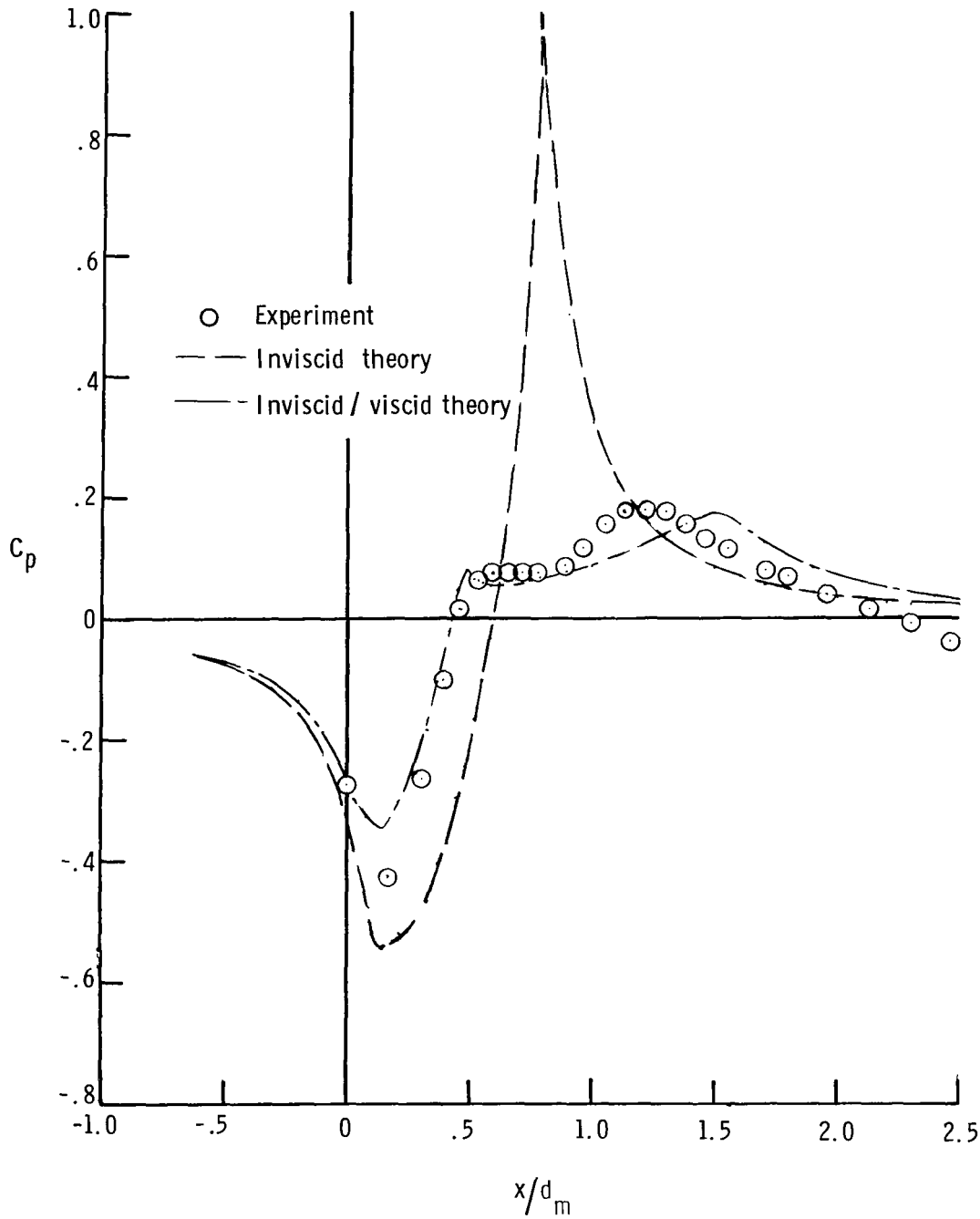

Figure 19.- Comparison of experimental and predicted pressure distributions on circular-arc boattail nozzle with Presz cone-frustum model representing separated region. $M_\infty = 0.80$; $l/d_m = 0.80$; $d_e/d_m = 0.50$.

1. Report No.	2. Government Accession No.	3. Recipient's Catalog No.
NASA TP-1226		

4. Title and Subtitle	5. Report Date
BOUNDARY-LAYER SEPARATION ON ISOLATED BOATTAIL NOZZLES	August 1978
	6. Performing Organization Code
7. Author(s)	8. Performing Organization Report No.
William Kelly Abeyounis	L-12104
	10. Work Unit No.
9. Performing Organization Name and Address	505-04-13-01
NASA Langley Research Center Hampton, VA 23665	11. Contract or Grant No.
	13. Type of Report and Period Covered
12. Sponsoring Agency Name and Address	Technical Paper
National Aeronautics and Space Administration Washington, DC 20546	14. Sponsoring Agency Code

15. Supplementary Notes

The information presented in this paper was offered as a thesis in partial fulfillment of the requirements for the Degree of Master of Science, George Washington University, Washington, D.C., May 1977.

16. Abstract

An investigation at an angle of attack of 0° has been conducted in the Langley 16-foot transonic tunnel at free-stream Mach numbers from 0.40 to 0.95 to study the phenomenon of separated flow on a series of circular-arc afterbodies. Both high-pressure air and solid circular cylinders with the cylinder diameter equal to the nozzle-exit diameter were used to simulate jet exhausts. The results indicated that boundary-layer separation is most extensive on steep boattails at high Mach numbers. Changes in the jet total-pressure ratio (jet total pressure to free-stream static pressure) affected the extent of separation very little; however, comparison of the separation data obtained by using the two jet-simulation techniques indicated that entrainment associated with the presence of a jet had a significant effect on the extent of separation. The solid-simulator separation data were also used to evaluate the predictions of eight separation criteria.

17. Key Words (Suggested by Author(s))	18. Distribution Statement
Flow separation Nozzles	Unclassified - Unlimited Subject Category 02

19. Security Classif. (of this report)	20. Security Classif. (of this page)	21. No. of Pages	22. Price*
Unclassified	Unclassified	60	$5.25

* For sale by the National Technical Information Service, Springfield, Virginia 22161

NASA-Langley, 1978

3 1 1U,A, 080478 S00903DS
DEPT OF THE AIR FORCE
AF WEAPONS LABORATORY
ATTN: TECHNICAL LIBRARY (SUL)
KIRTLAND AFB NM 87117